NAVAL POSTGRADUATE SCHOOL

MONTEREY, CALIFORNIA

THESIS

DOPPLER-ONLY SYNTHETIC APERTURE RADAR

by

Cheng Lock Charles Chua

December 2006

Thesis Advisor: Brett Borden
Co-Advisor: Donald Walters

Approved for public release; distribution is unlimited

THIS PAGE INTENTIONALLY LEFT BLANK

REPORT DOCUMENTATION PAGE		Form Approved OMB No. 0704-0188

1. AGENCY USE ONLY *(Leave blank)*	2. REPORT DATE December 2006	3. REPORT TYPE AND DATES COVERED Master's Thesis

4. TITLE AND SUBTITLE Doppler-Only Synthetic Aperture Radar	5. FUNDING NUMBERS
6. AUTHOR(S) Cheng Lock Charles Chua	
7. PERFORMING ORGANIZATION NAME(S) AND ADDRESS(ES) Naval Postgraduate School Monterey, CA 93943-5000	8. PERFORMING ORGANIZATION REPORT NUMBER
9. SPONSORING /MONITORING AGENCY NAME(S) AND ADDRESS(ES) N/A	10. SPONSORING/MONITORING AGENCY REPORT NUMBER

11. SUPPLEMENTARY NOTES The views expressed in this thesis are those of the author and do not reflect the official policy or position of the Department of Defense or the U.S. Government.

12a. DISTRIBUTION / AVAILABILITY STATEMENT Approved for public release; distribution is unlimited	12b. DISTRIBUTION CODE

13. ABSTRACT (maximum 200 words)

SAR has traditionally been performed using high-range resolution data. This thesis is a proof-of-concept that the imaging process can be performed using high-doppler resolution data. The system requires a simple continuous wave transmitter, and the signal returns are confined to a narrow band.

High-doppler resolution data is collected along an isodoppler line for different perspectives of the target. This data, a sinogram, is equivalent to taking the Radon transform of the target. The Fourier transform of the sinogram from each perspective (at an angle θ) gives a slice of the two-dimensional transform subtending an angle θ with the axis, with equally distributed points along the line. This results in a higher density of points near the centre. Some form of weighting is necessary. This weighting is part of the Filtered Backprojection algorithm to determine the Inverse Radon transform of the sinogram. The backprojection portion is a simple redistribution of data back along the original projection line.

Images were modeled by delta functions to test the above algorithm. The main points noted were that the reconstructed image was a scaled version of the original image, and that the quality of the image improved when more perspectives of the target were taken.

14. SUBJECT TERMS High Doppler Resolution, Radar Imaging	15. NUMBER OF PAGES 87
	16. PRICE CODE

17. SECURITY CLASSIFICATION OF REPORT	18. SECURITY CLASSIFICATION OF THIS PAGE	19. SECURITY CLASSIFICATION OF ABSTRACT	20. LIMITATION OF ABSTRACT
Unclassified	Unclassified	Unclassified	UL

NSN 7540-01-280-5500 Standard Form 298 (Rev. 2-89)
Prescribed by ANSI Std. 239-18

THIS PAGE INTENTIONALLY LEFT BLANK

Approved for public release; distribution is unlimited

DOPPLER-ONLY SYNTHETIC APERTURE RADAR

Cheng Lock Charles Chua
Major, Republic of Singapore Air Force
Bachelor of Engineering (Mechanical), National University of Singapore, 2000

Submitted in partial fulfillment of the
requirements for the degree of

MASTER OF SCIENCE IN COMBAT SYSTEMS SCIENCES AND TECHNOLOGY

from the

NAVAL POSTGRADUATE SCHOOL
December 2006

Author: Cheng Lock Charles Chua

Approved by: Brett Borden
Thesis Advisor

Donald Walters
Second Reader

James Luscombe
Chairman, Department of Physics

THIS PAGE INTENTIONALLY LEFT BLANK

ABSTRACT

SAR has traditionally been performed using high-range resolution data. This thesis is a proof-of-concept that the imaging process can be performed using high-doppler resolution data. The system requires a simple continuous wave transmitter, and the signal returns are confined to a narrow band.

High-doppler resolution data is collected along an isodoppler line for different perspectives of the target. This data, a sinogram, is equivalent to taking the Radon transform of the target. The Fourier transform of the sinogram from each perspective (at an angle θ) gives a slice of the two-dimensional transform subtending an angle θ with the axis, with equally distributed points along the line. This results in a higher density of points near the centre. Some form of weighting is necessary. This weighting is part of the Filtered Backprojection algorithm to determine the Inverse Radon transform of the sinogram. The backprojection portion is a simple redistribution of data back along the original projection line.

Images were modeled by delta functions to test the above algorithm. The main points noted were that the reconstructed image was a scaled version of the original image, and that the quality of the image improved when more perspectives of the target were taken.

THIS PAGE INTENTIONALLY LEFT BLANK

TABLE OF CONTENTS

I. INTRODUCTION....1
A. DOPPLER-ONLY SYNTHETIC APERTURE RADAR....1
B. OBJECTIVE....2
C. THESIS ORGANISATION....2

II. IMAGING RADAR BACKGROUND....5
A. TARGET RECOGNITION OVERVIEW....5
B. TARGET RECOGNITION TECHNIQUES....6
1. Cooperative Targets....6
2. Non-Cooperative Targets....6
3. Techniques....6
C. TARGET RECOGNITION IMPLEMENTATION....7
1. Recognition Based on Target Dynamics....7
2. Recognition Based on Target Structure....8
D. RADAR IMAGING....9
1. Imaging Radar Overview....9
2. Radar Images....9
3. Factors Affecting Backscatter....10
E. ONE-DIMENSIONAL IMAGING....11
1. Imaging with High Range Resolution Radar....11
2. Perceptual Classification....11
3. Implementation of High Range Resolution Techniques....12
F. TWO-DIMENSIONAL IMAGING....14
1. Synthetic Aperture Radars....14
2. Inverse Synthetic Aperture Radars....15
3. SAR and ISAR Comparisons....16
G. SAR APPLICATIONS....17
1. Treaty Verification and Non-Proliferation....17
2. Navigation and Guidance....18
3. Reconnaissance, Surveillance, and Targeting....19
4. Interferometry (3-D SAR)....19
5. Foliage and Ground Penetration....20
6. Moving Target Indication....21
7. Change Detection....22
8. Environmental Monitoring....23

III. HIGH DOPPLER RESOLUTION SAR....25
A. INTRODUCTION TO HIGH DOPPLER RESOLUTION SAR....25
B. DOPPLER RELATIONSHIPS....25
1. Doppler Definitions....25
2. Isodoppler Contours....28
C. CURRENT USES OF DOPPLER IMAGING....30
D. ANALOGY BETWEEN HRR SAR AND HDR SAR....30

1. Image Formation Based on HRR Data 30
2. Image Formation Based on HDR Data 33
E. MATHEMATICAL APPROACH TO HDR SAR 34
1. Radon Transform and Tomography 35
2. Projection Slice Theorem 37
3. Reconstruction by Filtered Backprojection 38
IV. IMPLEMENTATION OF DOPPLER IMAGING 41
A. SCENARIO SETUP 41
B. SIGNAL ANALYSIS FOR DOPPLER-ONLY SAR 44
C. EXTRACTING THE RADON TRANSFORM OF THE TARGET 44
1. Short-Time Fourier Transform 45
2. Illustration of STFT with Sinusoidal Signals 46
3. Sinogram of a Delta Function 48
D. INVERSE-RADON TRANSFORM 50
1. Filtering Process 51
2. Backprojection Process 52
3. Mathematical Implementation of the Filtered Backprojection 52
V. RESULTS AND FUTURE WORK 55
A. RESULTS 55
1. Basic Reconstruction Results 55
2. Discussion of Results 58
B. FUTURE WORK 59
1. More Complex Scenarios 59
2. Resolution Analysis 60
3. Performance in Real Environment 60
VI. SUMMARY AND CONCLUSION 61
A. SUMMARY 61
B. CONCLUSION 63
APPENDIX 65
LIST OF REFERENCES 69
INITIAL DISTRIBUTION LIST 71

LIST OF FIGURES

Figure 1 Return signal corresponding to individual target scatterers computed using a CAD model at High Range Resolution (From Ref. [8]) 12
Figure 2 ISAR image improvement with motion compensation (From Ref. [11]) 16
Figure 3 Satellite Image of North Korea Nuclear Facility (From Ref. [16]) 18
Figure 4 High Resolution SAR (above), compared to the optical image, to distinguish military targets (From Ref. [7]) 19
Figure 5 Three-dimensional terrain image from Interferometric SAR (From Ref. [7]) 20
Figure 6 Foliage Penetration using SAR (From Ref. [17]) 20
Figure 7 Underground bunker detection with ground penetrating SAR (From Ref. [18]) 21
Figure 8 Moving Target Indication extracted from SAR (From Ref. [7]) 22
Figure 9 Coherent Change Detection of vehicle tracks extracted from SAR (left) compared to the optical image (From Ref. [7]) 22
Figure 10 SAR image of Oil Seepage (From Ref. [7]) 23
Figure 11 Bistatic Doppler Geometry 26
Figure 12 Bistatic target doppler for stationary transmitter, stationary receiver, and a moving target 27
Figure 13 Isodoppler Contours from Bistatic radar (From Ref. [14]) 29
Figure 14 Ambiguity scenario due targets lying on lines of constant range from radar 31
Figure 15 Down-range and cross-range information facilitates image reconstruction 32
Figure 16 Different “slices” of the target when using HRR (left) and HDR 34
Figure 17 Concept of Line Integrals and the Radon Transform 35
Figure 18 Radon Transform of *f(x,y)* based on Parallel Projections 36
Figure 19 Graphical illustration of Projection Slice Theorem 38
Figure 20 Aircraft flying a circular path enclosing a non-centered target at time *t* 41
Figure 21 ISAR scenario which is mathematically similar to the SAR one in Figure 20 43
Figure 22 Sinogram of signal *x(t)* with a wide window and high frequency resolution 47
Figure 23 Sinogram of signal *x(t)* with a narrow window and high time resolution 47
Figure 24 Sinograms of delta functions at various locations on a 100x100 grid 49
Figure 25 Sinograms of a pair of delta functions at (10,10) and (60,60) 50
Figure 26 Data points evenly spaced along a spoke result in higher density of points near the centre 51
Figure 27 Overview of the reconstruction process (After [25]) 54
Figure 28 Image reconstruction of three delta functions in a straight line (upper left), and individual images of each of the three delta functions 55
Figure 29 Sinogram (top) and reconstructed image of three point-scatterers 56
Figure 30 Image reconstruction based on 45°, 90°, 135° and 180° (starting clockwise from top-left picture) views of the target 57
Figure 31 Effect of taking different number of perspectives of the target 57

Figure 32 Resolution limit when delta functions are separated by 30 units.....59
Figure 33 Summary of the image reconstruction process (After [25]) 61

LIST OF TABLES

Table 1 Capabilities of Short Pulse, High Range Resolution Radar (After Ref. [15]).....13

Table 2 Characteristics of Pulse Compression implemented by Linear Frequency Modulation and Binary Phase-Coded Pulses (After Ref. [15]) 13

Table 3 Effect of Geometry on Doppler Frequency (From Ref. [13]).....28

THIS PAGE INTENTIONALLY LEFT BLANK

ACKNOWLEDGMENTS

The whole process of choosing, doing and writing this thesis has been such a smooth one due in no small part to the countless contributions from many individuals. It has been a joy working with the NPS community, including professors, United States students and other foreign nationals, service and support staff from various departments (especially those at the library and student administration), and of course fellow Singaporeans.

To my thesis advisor, Professor Brett Borden, many thanks for the guidance, patience and direction throughout this journey. There were many simple and basic concepts that required explanation and insight, there were programming bugs that were just waiting to be discovered, and there were many seemingly dead-ends where I was lost and in need of a "sign," and you have provided all these. It is without doubt that this thesis would not have been completed if not for your professional and personal attention.

Professor Donald Walters has not only been my thesis co-advisor, but a dedicated lecturer for many classes as well. Your clarifications and descriptions have helped tremendously towards grasping difficult and abstract concepts.

To my wife and confidante, Valerie, I cannot begin to describe what a pillar you have been throughout our time in Monterey. You have looked after our family so well, especially our son Dominic, that we hardly fell sick and are all benefiting from the education system and living environment here. Our lives are made so fulfilling by what you have done, with what you have shared, and through your very presence. Thank you so very much. This thesis is dedicated to you.

THIS PAGE INTENTIONALLY LEFT BLANK

I. INTRODUCTION

A. DOPPLER-ONLY SYNTHETIC APERTURE RADAR

In conventional synthetic aperture radars or inverse synthetic aperture radars, the radar imaging process is based on collecting and processing high-range resolution data. Thus, it is conceptually viable that such an imaging process can also be performed using high-doppler resolution data only. This is the subject of this thesis.

The concept of doppler imaging is not entirely new. Doppler-only imaging has been applied to radar based planetary imaging, but it appears that this work is restricted to very limited geometries [26]. The reconstruction of a scattering density function from its integral over hyperbolas has also been developed [21] for wideband range-doppler radar imaging. Doppler imaging of a planar surface, however, has not been found to be studied in its own right.

The advantages of imaging based on high-doppler resolution are conceivably straightforward. The imaging system requires only a relatively simple and inexpensive continuous wave transmitter. The signal returns are inherently confined to a narrow band as doppler shifts are expected to be in the region of tens to hundreds of kilohertz. Conversely, pulse radars, due to the requirement for narrow pulses, will have a correspondingly larger bandwidth. The narrow bandwidth characteristic of a doppler-only imaging system is especially useful for covert operations or operations where the frequency spectrum use is restrictive, as well as for low frequency operations such as ground or foliage penetration imaging systems.

With a doppler-only imaging system, the high-doppler resolution data collected can be processed in a similar manner (to that from high-range resolution data) to reconstruct the original image. The original image can be obtained via the mathematical procedure of tomographic reconstruction, a process that is perhaps better known in the Medical context of a Computed Axial Tomography (CAT) scan.

B. OBJECTIVE

The objective of this thesis is to develop a basic theory for a doppler-only imaging radar based on high-doppler resolution data. The physics behind the imaging process will be discussed, and the mathematical implementation of such an imaging scheme will also be examined. The result of the above analysis will be tested on simple test cases consisting of images made up of simple delta functions.

C. THESIS ORGANISATION

This thesis is divided into six chapters, organized as follows:

Chapter II introduces the concepts of imaging radars. It begins with a discussion on the need for imaging radars based on the requirement of target recognition. Target recognition is further explored in terms of cooperative and non-cooperative types of targets, followed by various implementation approaches based on target dynamics or target structure. Subsequently, radar imaging is described with reference to one-dimensional and two-dimensional imaging concepts. In one-dimensional imaging using high-range resolution, simple perceptual classification can be obtained, and the characteristics of such an implementation via the transmission of short pulses are explained. In two-dimensional imaging, the concepts of synthetic aperture and inverse synthetic aperture radars are introduced, and comparisons are made. Applications of synthetic aperture radar are also discussed.

Chapter III puts forward the notion of doppler-only synthetic aperture radars. Comparisons and analogies between high-range resolution and high-doppler resolution techniques are used to explain the physics behind the doppler-only imaging methodology. An overview of the mathematical approach towards image formation using high-doppler resolution data is also provided.

Chapter IV extends the mathematical approach towards doppler imaging to an actual implemented scheme using simulated data. The implementation involved Radon transforms, Short-Time Fourier transforms, Projection Slice Theorems, and Inverse Radon transforms using Filtered Backprojection. The simulation data is based on imaging

a basic image made up of a series of delta functions. This chapter also includes a detailed explanation of the mathematical implementation of the doppler imaging concept.

Chapter V examines the results obtained from the doppler-only imaging process based on high-doppler resolution data. Based on these results, the scope of future work on this subject is then crafted.

Finally, Chapter VI summaries the whole process of the doppler-only image formation process using high-resolution doppler data, and concludes with some comments on the impetus towards developing a high-doppler resolution imaging system.

THIS PAGE INTENTIONALLY LEFT BLANK

II. IMAGING RADAR BACKGROUND

A. TARGET RECOGNITION OVERVIEW

Early radars were basically target detectors. They were able to detect the presence of a target and provide its location in range and azimuth, but offered little in addition to these basic data. As radar resolution improved in down-range and cross-range, it became possible to discern more information about the target. Finer resolution of the target was achieved by resolving the scattering centers of the target. What was previously just a "blob" of echo returns on the radar display can now include details on the very nature of the target to varying degrees.

The various degrees of target recognition, in increasing order of information required, can be classified as follows [1]:

- *General Nature of Target*: Based on simple characteristics of the echo return, such as strength, velocity and location of echo, a trained radar operator may be able to broadly classify the target echo as a return from an aircraft, ship, motor vehicle, rain, chaff, turbulence, land clutter, sea clutter or other natural phenomena.
- *Target Type*: A higher degree of classification that allows recognition of a fighter aircraft from a multi-engine transport aircraft, a cargo ship from a tanker, a tank from a truck and chaff rather than a ship.
- *Target Class*: This form of classification provides the exact class of platform that the target belongs to amongst many other similar platforms. If the target type is an aircraft, then classification of target class means distinguishing between an F-16, a MiG-29 or something similar. If the target type is a ship, then classification of target class means distinguishing between an Arleigh Burke Class Destroyer, a Baynunah Class Missile Corvette, or something similar.

The goal of the target recognition process is to extract as much information from the target as possible. In addition to the target details such as nature, type and class mentioned above, other relevant information may include the target's name, intention or its serial number! Recognition up to this fine level of detail may be termed Target Identification. This additional information may be especially important in the field of Air Traffic Control to correctly identify civil air liners in crowded airspace, such as in the vicinity of an airport. In the military context, target recognition and identification is a key step in the formulation of response plans and determining the next course of action.

B. TARGET RECOGNITION TECHNIQUES

1. Cooperative Targets

Full identification of a target usually requires some form of cooperation from the target itself. Common cooperative identification systems include the Identify Friend or Foe (IFF) system. In this case, the target must carry an IFF transponder, which will communicate with the IFF interrogator at a base station. With such a two-way communication system, aircraft or ships (where such systems area predominantly used) can identify themselves with a control centre to prevent any unnecessary response plans that may be activated against an unidentified platform. For civil aviation purposes, the IFF system provides an invaluable aid for identification and subsequent comparison to a database where the flight information of the civil airliner can be accessed.

2. Non-Cooperative Targets

Not every target will want to carry an IFF transponder to announce its presence and declare its full intention. Military targets, especially, fall into this category. When attempting to identify non-cooperative targets, other methods have to be used. These Non-Cooperative Target Recognition (NCTR) techniques are based on careful examination of the characteristics of the radar echo signal received from the target.

3. Techniques

Radar target recognition techniques tend to fall into two principle classes [2]: those that exploit the radar characterization of a platform's physical shape and those that exploit the radar characterization of the dynamic characteristics of the moving parts of the target. The former are based on the platform's (essentially instantaneous) range (time)-amplitude radar signature and are exploited through generation and analysis of the platform's High Range Resolution (HRR) profile. The latter are based on the platform's frequency-amplitude radar signature as represented in the time evolution of its high-resolution doppler signature.

The choice and implications of radar parameters, signal processing techniques, and pattern recognition techniques depends on the type of target. For example, ships are

generally easier to sort by class since ships contain more individual scatters that may be used to distinguish one class from another. Target classification generally requires a higher signal-to-noise ratio than target identification since detection depends on the total signal energy, but target recognition depends on discerning the details of the target echo signature. Thus, the characteristics of multiple small scatters from a target are critical for target recognition, whilst the returns from a few large scatterers might be sufficient to enable a generic detection of the target.

C. TARGET RECOGNITION IMPLEMENTATION

There are two steps towards implementing a target recognition process. The first is to distinguish the target echo from it surroundings. The useful radar echo signal that contains information about unique features of the target could be buried in noise and background clutter. The second aspect is the method by which a decision is made about the class, type or identification of the target based on analysis of the radar echo signal. This process is usually automated in conjunction with Decision Support Systems (DSS). A basic methodology upon which a DSS [3] for target recognition works is comparison of the received radar echo with a known database or library of signatures. The study of DSS in relation to target recognition is a separate field in itself with its own complexities, and will not be considered in this thesis.

1. Recognition Based on Target Dynamics

A well developed field for radar-based NCTR is the recognition of targets based on characterizations of radar signature in the doppler domain [2]. The techniques rely on high resolution doppler signatures of the target. The kinematics and phenomenology based characteristics of the target are extracted from either a single collected doppler signature, or a time evolution of doppler signatures. Short term features are usually found by analyzing the individual spectra via a Fast Fourier Transform (FFT). Longer term and periodically-appearing features are usually found by analyzing the time evolution of sequential FFTs of the doppler signature.

Key radar parameters relating to the accurate representation of kinematic attributes of the radar signature include: radar Pulse Repetition Frequency (PRF), Time-

On-Target (TOT), and FFT length. PRF determines the maximum unambiguous doppler that can be recorded and should be chosen so that all potentially important attributes may be distinctly separated. TOT determines the time available for observing important evolutions of the doppler signature, and should thus be chosen to be sufficiently long to encompass any such evolutions. FFT length determines the spectral resolution, and should thus be chosen to be able to resolve important doppler features. Ideally, a high PRF waveform with long time-on-target using multiple FFT lengths will optimize the target recognition process. However, such features will mean a compromise in a shorter unambiguous range, reduced coverage capabilities and complex signal processing respectively. This delicate balance is part of the radar design process, and must be kept in mind when performing numerical simulations for proof of concepts.

2. Recognition Based on Target Structure

Targets are normally distinguished from clutter based on doppler and/or amplitude information contained in the backscattered signal. Stationary targets are better analytical candidates when examining the amplitude domain. An optimal classical approach to Stationary Target Indication (STI) includes utilizing radar resolutions comparable to the sizes of the targets of interest, look times optimized to take advantage of the differing correlation times of the clutter and target of interests, frequency agility to speed clutter decorrelation, and some form of Constant False Alarm Rate (CFAR) processing of the coherent amplitude returns [9]. It has also been found that these domains often do not contain sufficient information to provide the levels of discrimination required for rigorous STI applications.

Another method is to analyze the full Polarization Scattering Matrix (PSM) of the target. This method can potentially measure all the information that can be contained in a backscattered radar waveform, but would require two transmit pulses per look and a dual channel receiver. Such a method has been demonstrated to be able to distinguish different types of targets from clutter based on their polarimetric properties even when the relative amplitudes of the signal returns are equal. Typical feature domains considered include polarimetric phase, Huynen parameters, and the Mueller matrix and Poincare sphere representations of the full PSM [10].

D. RADAR IMAGING

1. Imaging Radar Overview

An imaging radar works very much like a flash camera in that it provides its own light to illuminate an area on the ground and take a snapshot picture – but at radio wavelengths. A flash camera sends out a pulse of light (the flash) and records on film the light that is reflected back at it through the camera lens. Instead of a camera lens and film, a radar uses an antenna and digital computer tapes to record its images. In a radar image, one can see only the light that was reflected back towards the radar antenna.

Radar systems measure the strength and round-trip time of the microwave signals that are emitted by a radar antenna and reflected off a distant surface or object. The radar antenna alternately transmits and receives pulses at particular microwave wavelengths and polarizations. At the Earth's surface, the energy in the radar pulse is scattered in all directions, with some reflected back toward the antenna. This backscattered field returns to the radar as a weaker radar echo and is received by the antenna in a specific polarization. These echoes are converted to digital data and passed to a data recorder for later processing and display as an image. The radar pulse travels at the speed of light, and it is relatively straightforward to use the measured time for the roundtrip of a particular pulse to calculate the distance or range to the reflecting object. The chosen pulse bandwidth determines the resolution in the range (cross-track) direction. Higher bandwidth means finer resolution in this dimension. The length of the radar antenna determines the resolution in the azimuth (along-track) direction of the image: the longer the antenna, the finer the resolution in this dimension.

2. Radar Images

Radar images are composed of many dots, or picture elements [4]. Each pixel (picture element) in the radar image represents the radar backscatter for that area on the ground: darker areas in the image represent low backscatter, brighter areas represent high backscatter. Bright features mean that a large fraction of the radar energy was reflected back to the radar, while dark features imply that very little energy was reflected. Fractional backscatter, better known as radar cross section, for a target area at a particular

wavelength will vary for a variety of conditions: size of the scatterers in the target area, moisture content of the target area, polarization of the pulses, and observation angles. Backscatter will also differ when different wavelengths are used.

A useful rule-of-thumb in analyzing radar images is that the higher or brighter the backscatter on the image, the rougher the surface being imaged. Flat surfaces that reflect little or no microwave energy back towards the radar will always appear dark in radar images. Vegetation is usually moderately rough on the scale of most radar wavelengths and appears as grey or light grey in a radar image. Surfaces inclined towards the radar will have a stronger backscatter than surfaces which slope away from the radar and will tend to appear brighter in a radar image. Some areas not illuminated by the radar, like the back slope of mountains, are in shadows and will appear dark. When city streets or buildings are lined up in such a way that the incoming radar pulses are able to bounce off the streets and then bounce again off the buildings (called a double-bounce) and directly back towards the radar, they appear very bright (white) in radar images. Roads and freeways are flat surfaces so they appear dark. Buildings which do not line up so that the radar pulses are reflected straight back will appear light grey, like very rough surfaces.

3. Factors Affecting Backscatter

Backscatter will vary depending on the use of different polarization. Some imaging radars can transmit pulses in either horizontal (H) or vertical (V) polarization and receive in either H or V, with the resultant combinations of HH (Horizontal transmit, Horizontal receive), VV, HV, or VH. Additionally, some radars can measure the phase of the incoming pulse (one wavelength = 2π in phase) and therefore measure the phase difference in the return of the HH and VV signals. This difference can be thought of as a difference in the roundtrip times of HH and VV signals, and is frequently the result of structural characteristics of the scatterers. Imaging radars can also measure the correlation coefficient for the HH and VV returns, which can be considered as a measure of how alike the HH and VV scatterers are.

Different observation angles also affect backscatter. Track angle will affect backscatter from very linear features: urban areas, fences, rows of crops, ocean waves, fault lines, etc. The angle of the radar wave at the Earth's surface (called the incidence

angle) will also cause a variation in the backscatter: low incidence angles (perpendicular to the surface) will result in high backscatter; backscatter will decrease with increasing incidence angles.

E. ONE-DIMENSIONAL IMAGING

1. Imaging with High Range Resolution Radar

Radars with high range resolution (HRR) are able to resolve the individual scatterers of the target and provide a down-range profile of the target, as shown in Figure 1. This method essentially provides a one-dimensional image of the target. The down-range, or radial, profile is useful in obtaining an approximation of the length of the target, but this can be affected by a variety of factors such as aspect angle, position of the major scatterers or masking of the scatterers by other parts of the target. Awareness of these factors is critical when correlating imaging data with a library of reference profiles so as to increase the accuracy of target identification analysis. Range profile imaging is a conceptually straightforward idea, but implementation may be difficult [5] due to the multiple unknowns associated with the target, and the amount of referencing and comparisons required as the library of profiles will include many permutations due to different aspect angles, different classes of targets, and different types of targets within a class.

2. Perceptual Classification

The complexities described above have made it difficult to recognise specific targets from different classes. The information gathered from the one-dimensional range profile, however, has been shown to be able to separate targets into a simpler set of general classes [6]. This has been termed Perceptual Classification. Using an L-band radar with one metre resolution, air targets can be separated into the following general categories: small or large jet engine aircraft, small or large propeller aircraft, helicopters, and missiles.

Similarly, in the one-dimensional imaging of ships, sea targets can be separated into the following categories: large ships, small ships, military ships, commercial ships, tankers and aircraft carriers.

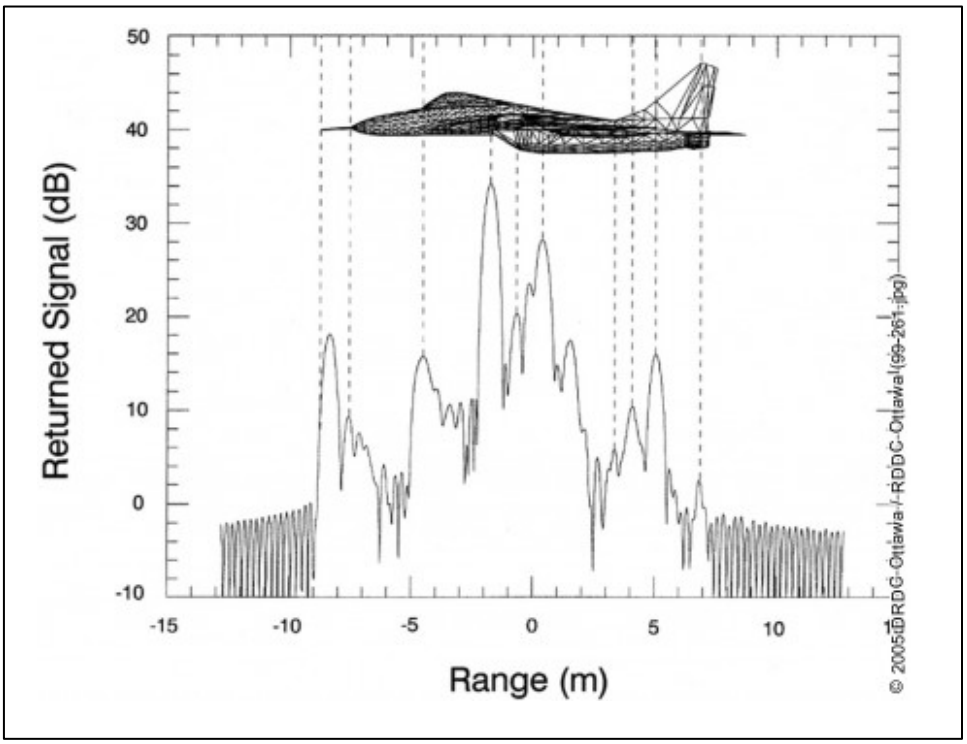

Figure 1 Return signal corresponding to individual target scatterers computed using a CAD model at High Range Resolution (From Ref. [8])

3. Implementation of High Range Resolution Techniques

Real aperture radar systems can be made to provide fine range resolution via the incorporation of high range resolution (HRR) techniques. The generation of HRR profiles are accomplished via the transmission of extremely short pulses or via some form of pulse compression. The generic capabilities of a short pulse, high range resolution radar are summarised in Table 1. The two more common techniques of pulse compression waveforms are Linear Frequency Modulation (LFM), also known as chirp, and binary phase-coded pulses [15]. These two techniques are compared in Table 2.

Range Resolution	Usually easier to separate (resolve) multiple targets in range than in angle.
Range Accuracy	Good range resolution will result in good range accuracy.
Clutter Reduction	Increased target-to-clutter ratio obtained by reducing amount of distributed clutter with which the target echo signal must compete.
Interclutter visibility	With some types of "patchy" land and sea clutter, a high-resolution radar can detect moving targets in the clear areas between the clutter patches.
Glint Reduction	Angle and range tracking errors of a complex target with multiple scatterers are reduced when high range resolution is employed to isolate (resolve) the individual scatterers that make up the target.
Multipath Resolution	Range resolution permits the separation of the desired target echo from other echoes that arrives at the radar via scattering from longer propagation paths, or multipath.
Multipath Height-Finding	When multipath due to scattering of radar energy from Earth's surface can be separated from the direct-path signal via range resolution, the target height can be determined without direct measurement of elevation angle.
Target Classification	Radial profile of a target can provide a measure of the target's radial dimension, and generic sorting of one type of target from another based on size or other distinct profile.
ECCM	A short pulse radar can negate the effects of certain electronic countermeasures such as range-gate stealers, repeater jammers and decoys.
Minimum Range	A short pulse allows the radar to operate with a short minimum range. It also allows the reduction of blind zones (eclipsing) in high pulse repetition frequency radar.

Table 1 Capabilities of Short Pulse, High Range Resolution Radar (After Ref. [15])

Property	**Linear Frequency Modulation**	**Binary Phase-Coded Pulses**
Time Sidelobes	Good (~30dB) when weighting on receive, and when a loss of about 1dB can be tolerated	Can equal $1/2N$, and are not easy to improve; poor doppler sidelobes
Doppler	Doppler tolerant	Requires filter bank
Pulse Compression Filter	Single filter can be used for transmit and receive; usually analog for high-resolution	Single filter can be used for transmit and receive, but with input at opposite end; usually digital
Complexity	Less complex	More complex, requires filter bank
Application	High-resolution (wide bandwidth)	Long pulses

Table 2 Characteristics of Pulse Compression implemented by Linear Frequency Modulation and Binary Phase-Coded Pulses (After Ref. [15])

There are limitations, however, for short pulses. Since the spectral bandwidth of a pulse is inversely proportional to its duration, the bandwidth of a short pulse is large. Large bandwidth can increase system complexity, make greater demands on the signal processing, and increase the likelihood of interference from other users of the electromagnetic spectrum. Wide bandwidth can also mean less dynamic range in the receiver because receiver noise power is proportional to bandwidth. Also, a short pulse waveform provides less accurate radial velocity measurement than if obtained from the doppler frequency shift. Finally, a serious limitation to achieving long ranges with short duration pulses is that a high peak power is required for large pulse energy. The transmission line of a high peak power radar can suffer voltage breakdown (arc discharge), especially at the higher frequencies where waveguide dimensions are small. If peak power is limited by breakdown, the pulse might not have sufficient energy.

F. TWO-DIMENSIONAL IMAGING

For reliable target classification, other information is usually needed in addition to the range profile. This added information can be the high-resolution cross-range profile, or doppler profile. The two-dimensional image of a target (based on down-range and cross-range profile) can be obtained by use of an imaging radar such as Synthetic Aperture Radar (SAR) and Inverse Synthetic Aperture Radar (ISAR).

1. Synthetic Aperture Radars

Synthetic Aperture Radar (SAR) refers to a technique used to synthesize a very long antenna by combining signals (echoes) received by the radar as it moves along its flight track. An aperture is the opening used to collect the reflected energy that is used to form an image. In the case of a camera, this would be the shutter opening; for radar it is the antenna. A synthetic aperture is constructed by moving a real aperture or antenna through a series of positions along the flight track.

As the radar moves, a pulse is transmitted at each position; the return echoes pass through the receiver and are recorded in an 'echo store.' Because the radar is moving relative to the ground, the returned echoes are doppler-shifted. Comparing the doppler-

shifted frequencies to a reference frequency allows many returned signals to be “focused” on a single point, effectively increasing the length of the antenna that is imaging a particular point. This focusing operation, commonly known as SAR processing, is now done digitally on fast computer systems. The trick in SAR processing is to correctly match the variation in doppler frequency for each point in the image: this requires very precise knowledge of the relative motion between the platform and the imaged objects (which is the cause of the doppler variation in the first place).

Synthetic aperture radar is now a mature technique used to generate radar images in which fine detail can be resolved. SAR can provide unique capabilities as an imaging tool. Since a SAR essentially provides its own illumination (the radar pulses), it can image at any time of day or night, regardless of sun illumination. As the radar wavelengths are much longer than those of visible or infrared light, SAR can also “see” through cloudy and dusty conditions that visible and infrared instruments cannot.

2. Inverse Synthetic Aperture Radars

In an Inverse Synthetic Aperture Radar (ISAR), the cross-range resolution can be considered to be obtained by means of high-resolution in the doppler, or frequency, domain. Since each part of the moving target will have a different relative velocity with respect to the radar, this difference in the doppler velocity will be used to resolve the cross-range resolution. Targets with a large rotational component will produce a greater doppler signature, and the cross-range resolution is dependant on the amount of angular rotation of the target during the radar observation time. The resolution in the down-range dimension is obtained via a short pulse, and thus, a two-dimensional image can be obtained.

SAR and ISAR are related in that they both require a change in the perspective of the target to produce the image. In SAR, the target is assumed stationary and the radar is in motion. In ISAR, the target motion provides the change in relative velocity, which results in differing doppler shifts to occur across the target.

For this reason, ships, which inherently have pitching, rolling and yawing motion, provide good targets for analysis using ISAR methods. The pitch motion of a ship causes

the top of the masts to have a higher velocity than the bottom of the masts or superstructure, thus providing a means to map its vertical profile along the length of the ship. The roll motion also provides height information, but in the plane that includes the width of the ship. The yaw motion provides a plan view of the target. As a ship pitches, rolls and yaws, ISAR might produce a combination of the abovementioned profiles that result in an image appearing as a perspective. However, as these angular rates of changes are not known, an accurate image cannot be formed. Additional methods have to be implemented to take into account how the pitch, roll and yaw motion are affected by external forces. One such method is motion compensation [11], where the motion of the target is estimated using measurable parameters from the external environment, and the improvements over the original ISAR image can clearly be seen as shown in Figure 2.

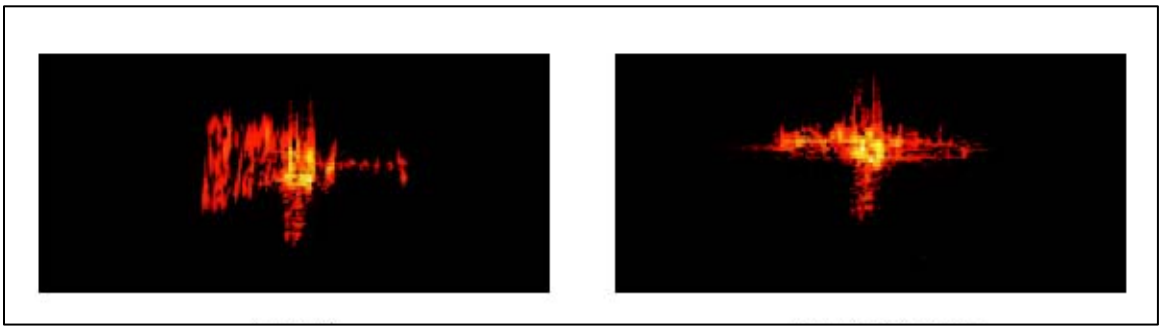

Figure 2 ISAR image improvement with motion compensation (From Ref. [11])

The classification of aircraft with ISAR is more difficult than utilising ISAR methods on ships. This is due to an aircraft having fewer scattering centres than a ship, and also since an aircraft does not have sufficient roll, pitch and yaw motions to isolate discrete scattering features important for target recognition.

3. SAR and ISAR Comparisons

In principle, SAR images are formed when data are collected over some spatial baseline, and then processed in such a way as to emulate an antenna spanning that baseline. ISAR images are formed in much the same way, expect that the emulated antenna baseline is formed on the basis of the movement of the target rather than the

sensor [10]. In both cases, images with relatively fine cross-range (azimuthal) resolution can be formed. Generally, it is advantageous to design the system so that its cross-range resolution matches its range resolution.

The principal advantage in utilising imaging rather than real aperture radar systems is the significant reduction of inter- and intra- cell clutter in the scene. The principal advantages in utilising imaging for classification and identification are the additional information provided due to the finer resolution of the output. For man-in-the-loop systems, the highly intuitive nature of an image is another advantageous factor for the imaging format. The principal disadvantages of SAR and ISAR imaging systems are the high time-on-target generally required, and in the case of automatic target recognition systems, the requisite processor complexity.

G. SAR APPLICATIONS

There are a variety of applications for SAR [7]. These applications increase almost daily as new technologies and innovative ideas are developed. While SAR is often used because of its all-weather, day-or-night capability, it also finds application because it renders a different view of a "target," with synthetic aperture radar being at a much lower electromagnetic frequency than optical sensors.

1. Treaty Verification and Non-Proliferation

The ability to monitor other nations for treaty compliance and for the non-proliferation of nuclear, chemical, and biological weapons is increasingly critical. Often, monitoring is possible only at specific times, when overflights are allowed, or it is necessary to maintain a monitoring capability in inclement weather or at night, to ensure that an adversary is not using these conditions to hide an activity. SAR provides the all-weather capability and complements the information available from other airborne sensors, such as optical or thermal-infrared sensors. SAR imagery provided invaluable assessments following North Korea's nuclear test in October 2006, as shown in Figure 3.

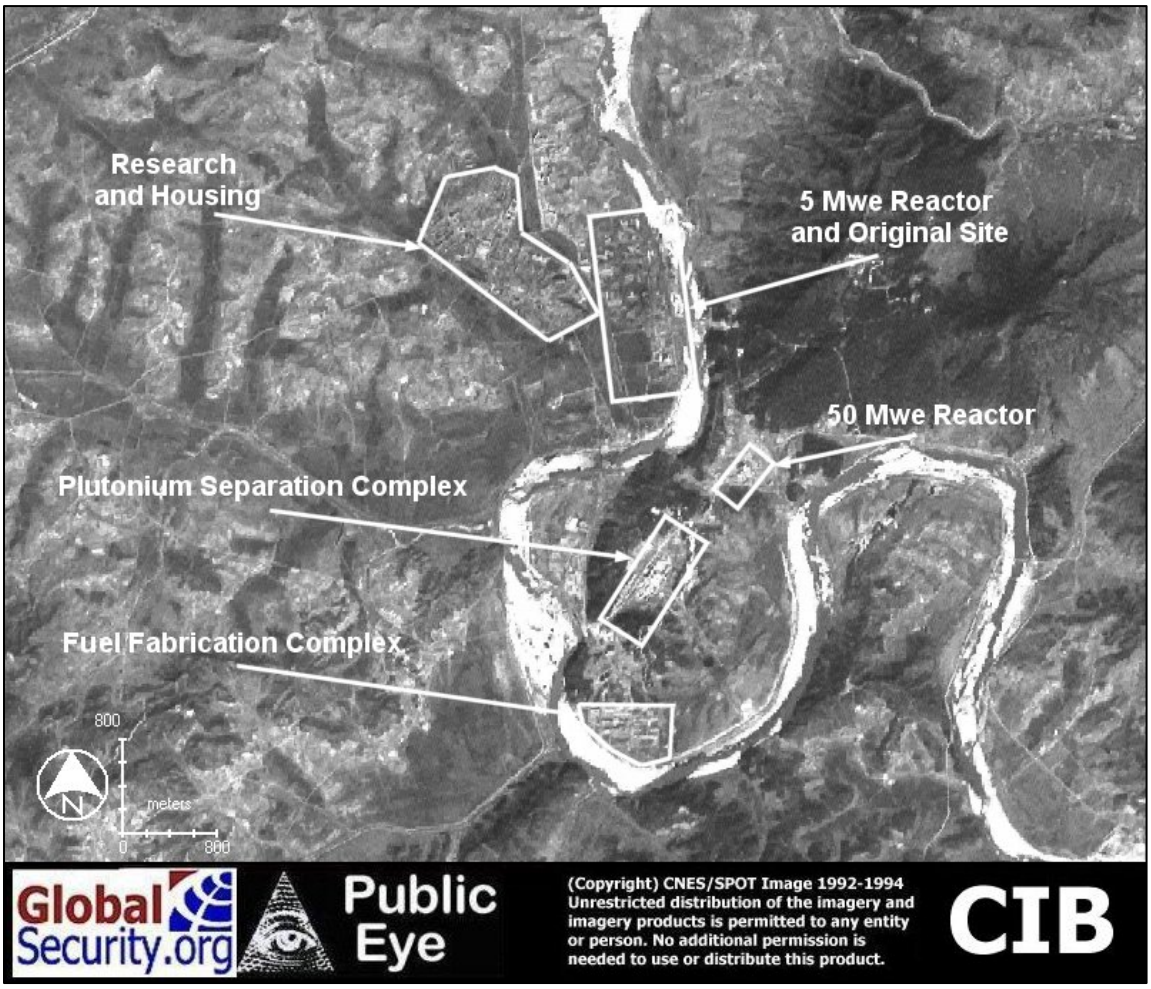

Figure 3 Satellite Image of North Korea Nuclear Facility (From Ref. [16])

2. Navigation and Guidance

Synthetic aperture radar provides the capability for all-weather, autonomous navigation and guidance. By forming SAR reflectivity images of the terrain and then "correlating" the SAR image with a stored reference (obtained from optical photography or a previous SAR image), a navigation update can be obtained. Position accuracies of less than a SAR resolution cell can be obtained. SAR may also be used in guidance applications by pointing or "squinting" the antenna beam in the direction of motion of the airborne platform. In this manner, the SAR may image a target and guide munitions with high precision.

3. Reconnaissance, Surveillance, and Targeting

Many applications of synthetic aperture radar are for reconnaissance, surveillance, and targeting. These applications are driven by the military's need for all-weather, day-and-night imaging sensors. SAR can provide sufficiently high resolution to distinguish terrain features and to recognize and identify selected man-made targets, as shown in Figure 4.

Figure 4 High Resolution SAR (above), compared to the optical image, to distinguish military targets (From Ref. [7])

4. Interferometry (3-D SAR)

Interferometric synthetic aperture radar (IFSAR) data can be acquired using two antennas on one aircraft or by flying two slightly offset passes of an aircraft with a single antenna. Interferometric SAR can be used to generate very accurate surface profile maps of the terrain as shown in Figure 5.

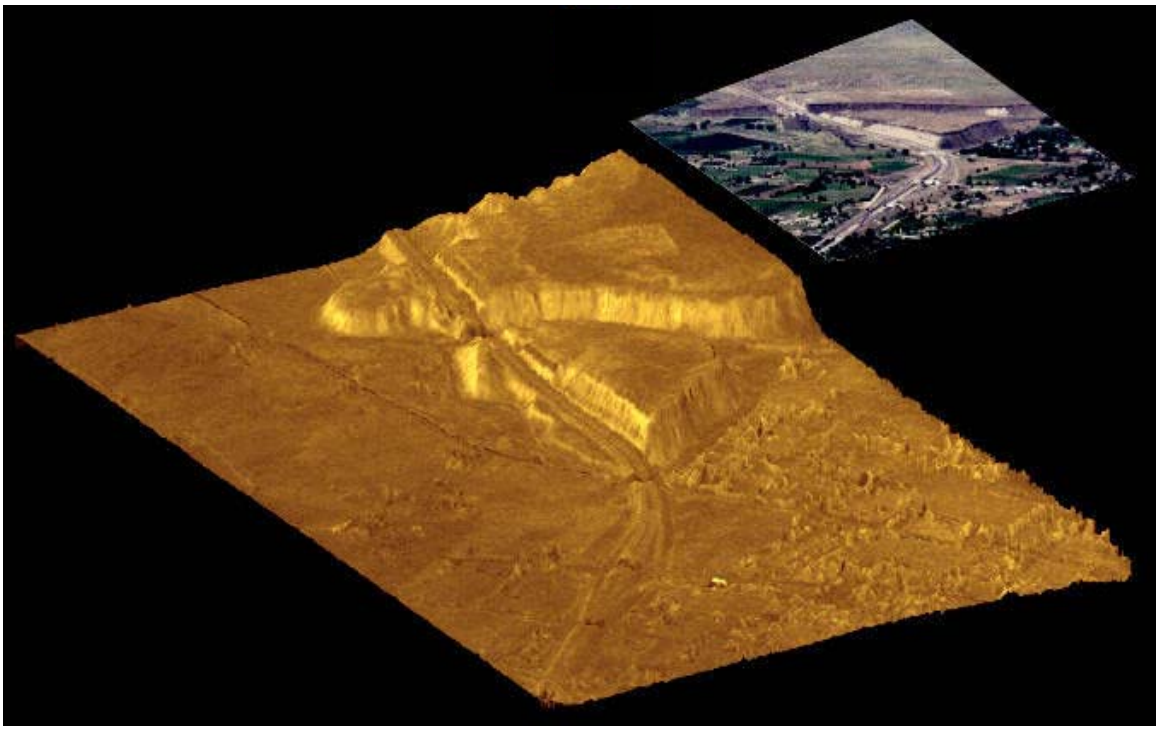

Figure 5 Three-dimensional terrain image from Interferometric SAR (From Ref. [7])

5. Foliage and Ground Penetration

Synthetic aperture radars offer the capability for penetrating materials which are optically opaque, and thus not visible by optical or IR techniques. Low-frequency SARs may be used under certain conditions to penetrate foliage and even soil. This provides the capability for imaging targets, normally hidden by trees, brush, and other ground cover as shown in Figure 6. To obtain adequate foliage and soil penetration, SARs must operate at relatively low frequencies (10's of MHz to 1 GHz).

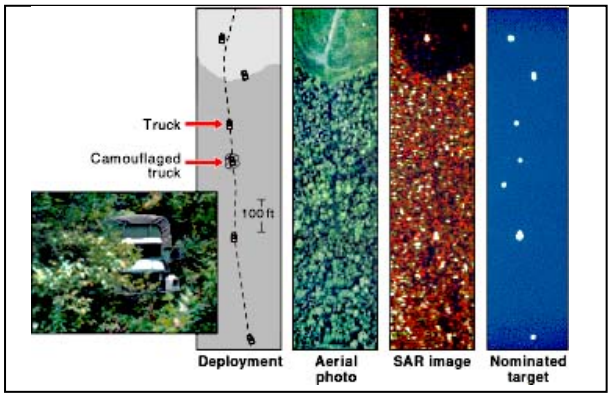

Figure 6 Foliage Penetration using SAR (From Ref. [17])

Recent studies have shown that SAR may provide a limited capability for imaging selected underground targets, such as utility lines, arms caches, bunkers and mines, as shown in Figure 7. Depth of penetration varies with soil conditions (moisture content, conductivity, etc.) and target size, but individual measurements have shown the capability for detecting 55-gallon drums and power lines at depths of several meters. In dry sand, penetration depths of 10's of meters are possible.

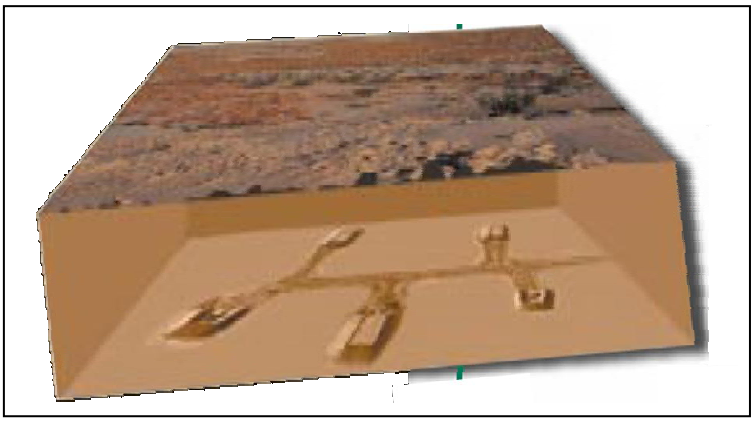

Figure 7 Underground bunker detection with ground penetrating SAR (From Ref. [18])

6. Moving Target Indication

The motion of a ground-based moving target such as a car, truck, or military vehicle, causes the radar signature of the moving target to shift outside of the normal ground return of a radar image. However, techniques have been developed to automatically detect ground-based moving targets and to extract other target information such as location, speed, size, and Radar Cross Section (RCS) from these target signatures, as shown in Figure 8.

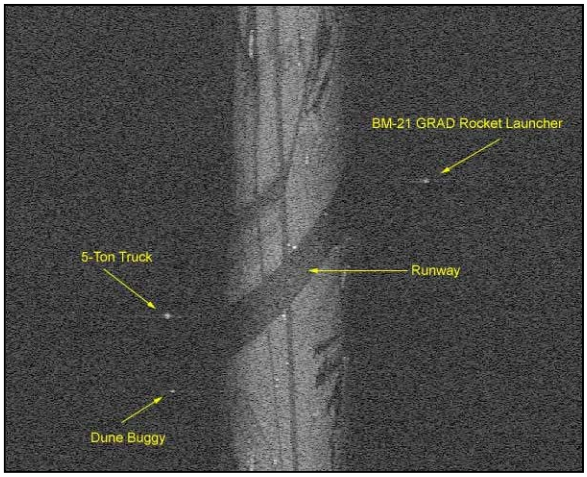

Figure 8 Moving Target Indication extracted from SAR (From Ref. [7])

7. Change Detection

Similarly, coherent change detection offers the capability for detecting changes between imaging passes. To detect whether or not a change has occurred, two images are taken of the same scene, but at different times. These images are then geometrically registered so that the same target pixels in each image align. After the images are registered, they are cross correlated pixel by pixel. Where a change has not occurred between the imaging passes, the pixels remain correlated, whereas if a change has occurred, the pixels are uncorrelated. This is illustrated in Figure 9.

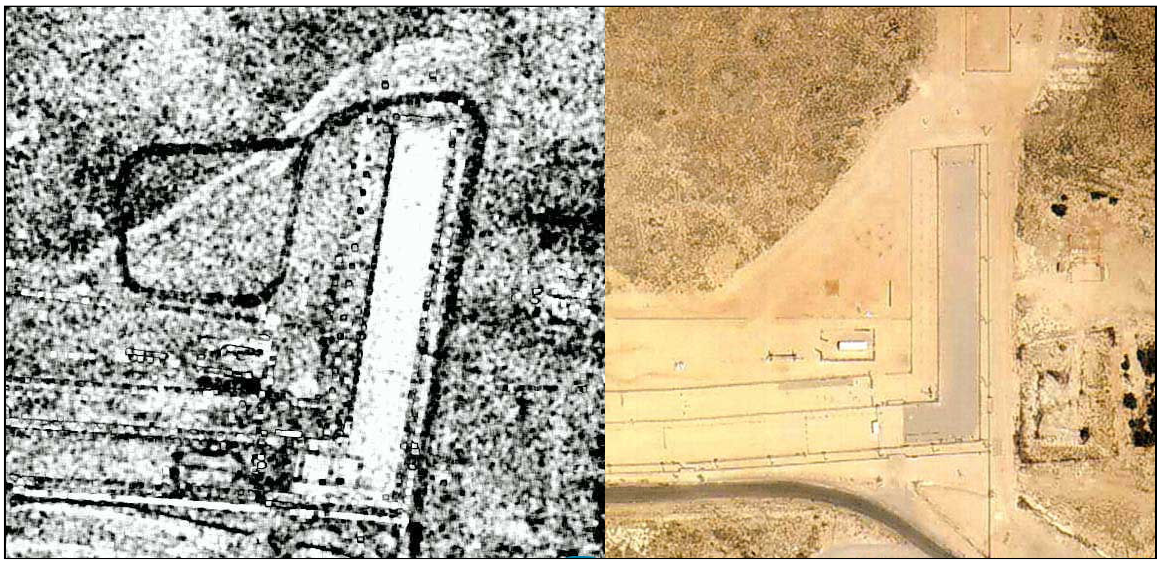

Figure 9 Coherent Change Detection of vehicle tracks extracted from SAR (left) compared to the optical image (From Ref. [7])

8. Environmental Monitoring

Synthetic aperture radar is used for a wide variety of environmental applications, such as monitoring crop characteristics, deforestation, ice flows, and oil spills. Oil spills can often be detected in SAR imagery because the oil changes the backscatter characteristics of the ocean. Radar backscatter from the ocean results primarily from capillary waves through what is known as Bragg scattering (constructive interference from the capillary waves being close to the same wavelength as the SAR). The presence of oil dampens the capillary waves, thereby decreasing the radar backscatter. Thus, the oil slicks appear dark in SAR images relative to oil-free areas in Figure 10.

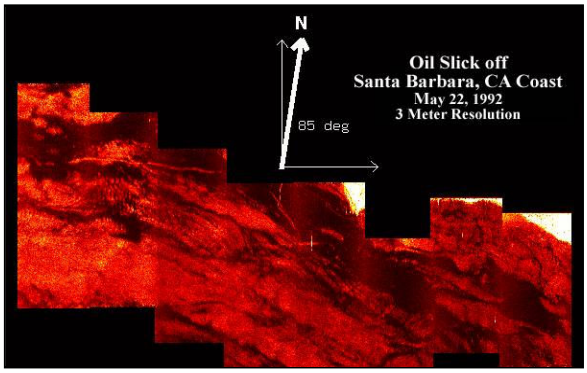

Figure 10 SAR image of Oil Seepage (From Ref. [7])

THIS PAGE INTENTIONALLY LEFT BLANK

III. HIGH DOPPLER RESOLUTION SAR

A. INTRODUCTION TO HIGH DOPPLER RESOLUTION SAR

Standard synthetic aperture radar imaging systems transmit high range resolution (HRR) waveforms and the radar returns are used to obtain estimates of the distances to the various scatterers of a target, thus mapping out the range profile of the target. With a HRR system, the radar return at each time step *t* is a superposition of all the returns from the scatterers at a distance *2t/c* from the radar. The imaging problem is formulated in terms of reconstructing the scattering density function ρ from it integrals over all circles centered on the flight path of the antenna.

The complementary system to the HRR imaging system is to transmit high-doppler resolution waveforms (such as fixed-frequency, continuous wave or CW waveform) in order to determine the relative target velocity from the doppler frequency shift of the radar return [12]. For an antenna moving at a constant velocity over a flat surface, the return at a given doppler shift is a superposition of all the returns due to scatterers with the same relative velocity lying along a hyperbola, termed the isodoppler curve. The imaging problem is thus to reconstruct the scattering density function from the integrals over the isodoppler hyperbolas.

B. DOPPLER RELATIONSHIPS

1. Doppler Definitions

A canonical definition of bistatic doppler, or doppler shift, f_B, is the time rate of change of the total path length of the scattered signal, normalised by the wavelength [13]. Since the total path length is the range sum $R_T + R_R$

$$f_B = \frac{1}{\lambda}\left[\frac{\mathrm{d}}{\mathrm{d}t}\left(R_T + R_R\right)\right]$$
$$= \frac{1}{\lambda}\left[\frac{\mathrm{d}R_T}{\mathrm{d}t} + \frac{\mathrm{d}R_R}{\mathrm{d}t}\right]$$

Figure 11 illustrates the geometry and kinematics for bistatic doppler when the target, transmitter and receiver are moving. The target's velocity vector projected onto

the bistatic place has magnitude V and aspect angle δ referenced to the bistatic bisector. The aspect angle is positive when measured clockwise from the bistatic bisector. The transmitter and receiver have projected velocity vectors of magnitude V_T and V_R, and aspect angles of δ_T and δ_R respectively.

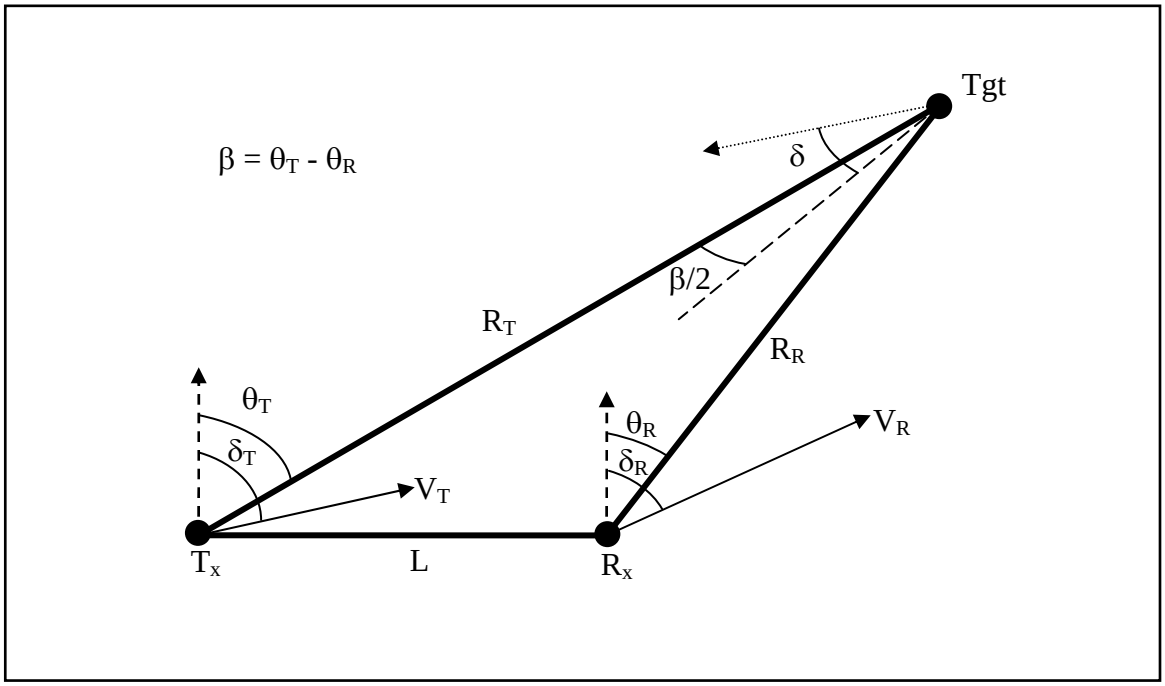

Figure 11 Bistatic Doppler Geometry

When the transmitter and receiver are stationary ($V_T = V_R = 0$) and the target is moving ($V \neq 0$), the target's bistatic doppler at the receiver site is developed as follows. The term dR_T/dt is the projection of the target velocity vector onto the transmitter-to-target line-of-sight:

$$\frac{dR_T}{dt} = V\cos\left(\delta - \frac{\beta}{2}\right)$$

Similarly, dR_R/dt is the projection of the target velocity vector onto the receiver-to-target line-of-sight:

$$\frac{dR_R}{dt} = V\cos\left(\delta + \frac{\beta}{2}\right)$$

Thus, the bistatic doppler shift caused only by target motion, f_{Tgt}, is given below and plotted in Figure 12 for three values of β.

$$
\begin{aligned}
f_B = f_{\mathrm{Tgt}} &= \frac{1}{\lambda}\left[\frac{\mathrm{d}R_T}{\mathrm{d}t} + \frac{\mathrm{d}R_R}{\mathrm{d}t}\right] \\
&= \frac{V}{\lambda}\left[\cos\left(\delta - \frac{\beta}{2}\right) + \cos\left(\delta + \frac{\beta}{2}\right)\right] \\
&= \frac{2V}{\lambda}\cos\delta\cos\left(\frac{\beta}{2}\right)
\end{aligned}
$$

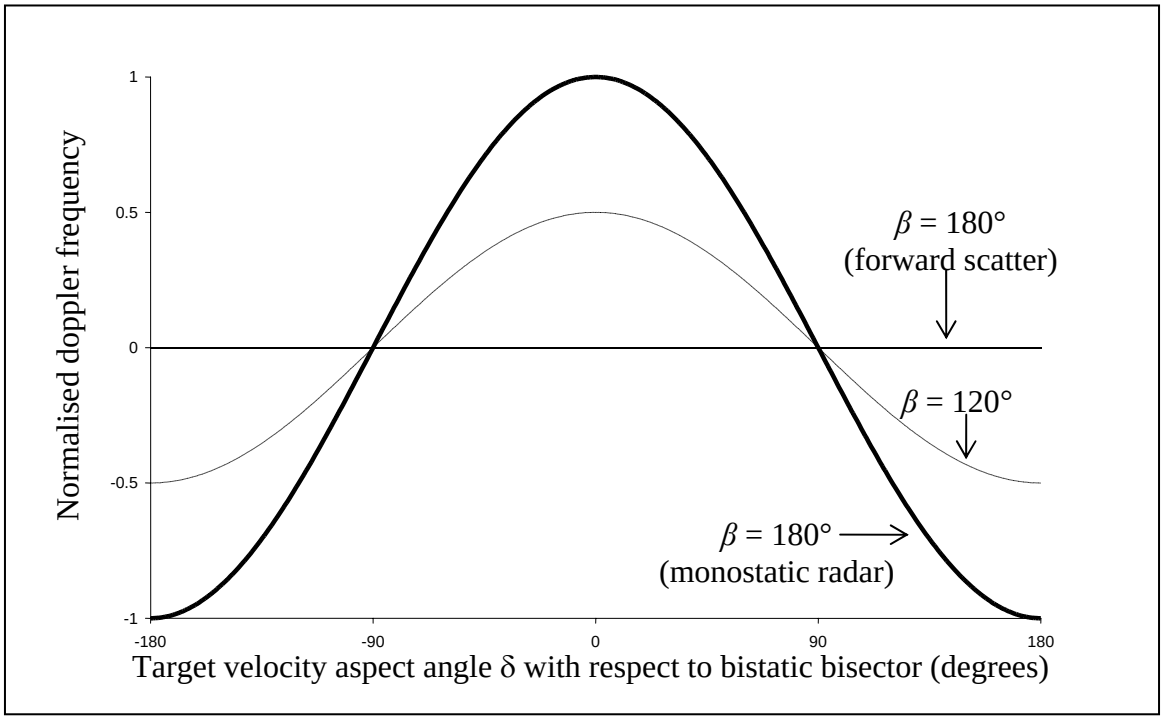

Figure 12 Bistatic target doppler for stationary transmitter, stationary receiver, and a moving target

With β=0°, the scenario is essentially the case of a monostatic radar located on the bistatic bisector, and δ is now the angle between the target velocity vector and the monostatic radar-to-target line-of-sight. When β=180°, we have the forward-scatterer case where $f_{\mathrm{Tgt}} = 0$ for any δ. For all β, when $-90° < \delta < 90°$, the bistatic target doppler is positive. This is the normal definition for positive doppler shift when the target is closing in towards the radar. For all β, when the target's velocity vector is normal to the bistatic

bisector, (δ = ±90°), the bistatic target doppler is zero. This vector is collinear with a tangent to an isorange contour drawn through the target position. Thus, all isorange contours are contours of zero bistatic target doppler. When there is no velocity component in the direction towards the radar, the target will not present a doppler signature to the radar. The geometry-dependent effects on the doppler are summarised in Table 3.

δ	f_{Tgt}	**Geometry**
$\beta/2$	$(2V/\lambda)\cos^2(\beta/2)$	V pointed at transmitter
$-\beta/2$	$(2V/\lambda)\cos^2(\beta/2)$	V pointed at receiver
0	$(2V/\lambda)\cos^2(\beta/2)$	V pointed down the bistatic bisector
±90°	0	V perpendicular to the bistatic bisector
180°	$-(2V/\lambda)\cos(\beta/2)$	V pointed out the bistatic bisector
$90\pm\beta/2$	$\mp(V/\lambda)\sin(\beta/2)$	V perpendicular to transmitter or receiver line-of-sight

Table 3 Effect of Geometry on Doppler Frequency (From Ref. [13])

2. Isodoppler Contours

When the target is stationary, and the transmitter and receiver are moving (as in the case of an airborne SAR), the bistatic doppler at the receiving site due to the combined transmitter and receiver motion is developed as follows. The terms dR_T/dt and dR_R/dt are now the projections of the transmitting and receiving velocity vectors onto their respective target line-of-sights. The doppler shift, f_{TR}, is thus:

$$f_B = f_{TR} = \frac{V_T}{\lambda}\cos(\delta_T - \theta_T) + \frac{V_R}{\lambda}\cos(\delta_R - \theta_R)$$

where f_{TR} is the bistatic doppler shift caused by the combined transmitter and receiver motion. In the monostatic case, with $V_T = V_R = V_M$, $\delta_T = \delta_R = \delta_M$, $\theta_T = \theta_R = \theta_M$, the monostatic doppler shift, f_M, for stationary target and moving transmitter/receiver is thus

$$f_M = \frac{2V_M}{\lambda}\cos\left(\delta_M - \theta_M\right)$$

where $\left(\delta_M - \theta_M\right)$ is the angle between the monostatic radar's velocity vector and the radar-to-stationary-target line-of-sight.

The locus of points for constant doppler shift on the Earth's surface is called an isodoppler contour. In the monostatic case with a flat earth, these isodopplers are conic sections in three dimensions, in which the cone is a consequence of the radar's beamwidth. In the bistatic case, the isodopplers are skewed, depending on the transmitting and receiving site kinematics, as defined by V_T, V_R, δ_T, and δ_R. These curves can be developed analytically for a simple case of a coplanar flat earth and bistatic plane by setting f_{TR} = constant and solving for θ_T or θ_R, as illustrated in Figure 13.

$$\theta_R = \delta_R \pm \cos^{-1}\left[\frac{f_{TR} - \left(\frac{V_T}{\lambda}\right)\cos\left(\delta_T - \theta_T\right)}{\frac{V_R}{\lambda}}\right]$$

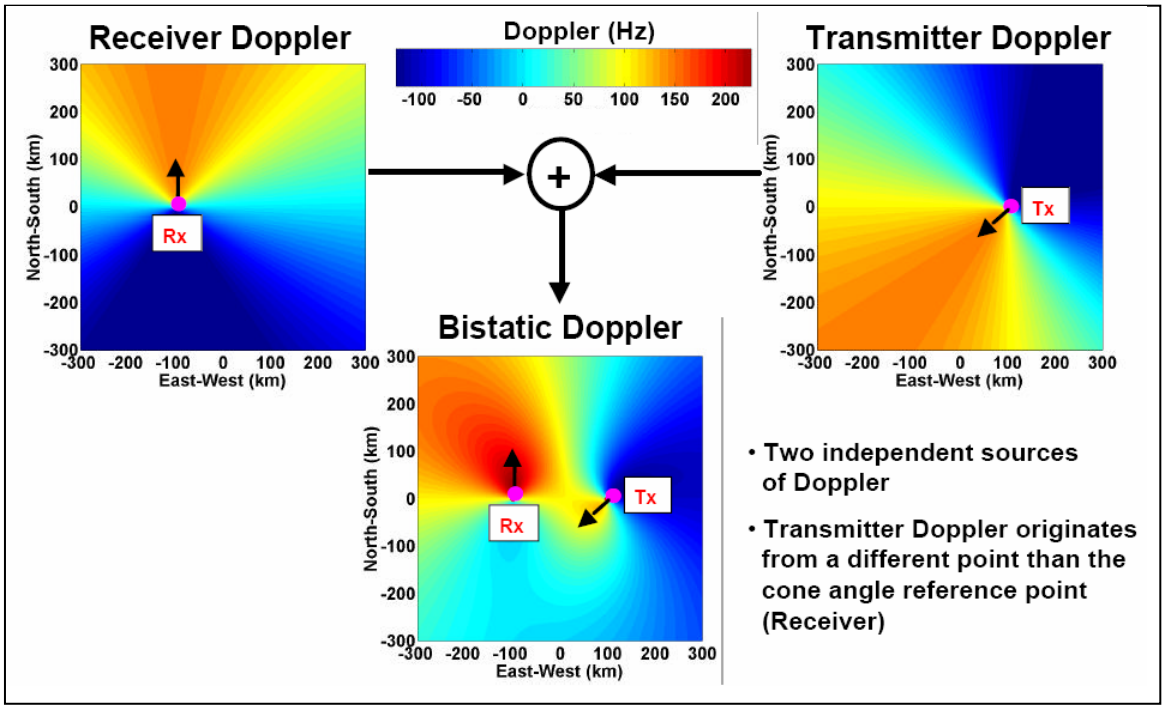

Figure 13 Isodoppler Contours from Bistatic radar (From Ref. [14])

C. CURRENT USES OF DOPPLER IMAGING

High doppler resolution (HDR) imaging systems require only a relatively simple (inexpensive) transmitter and may thus have advantages over high range resolution systems (HRR) in some situations. In addition, doppler imaging systems may be useful in scenarios in which the radar must penetrate through a medium with a frequency dependent attenuation.

The concept of doppler imaging appeared in [19] in the context of a rotating target and stationary radar to motivate the development of range-doppler or inverse synthetic aperture imaging. Doppler-only imaging has also been applied to radar-based planetary imaging [20]. The High Resolution Doppler Imager (HRDI) was one of the instruments on board the Upper Atmospheric Research Satellite used to observe the emission and absorption lines of molecular oxygen, as well as other atmospheric components, in small volumes above the limb of the Earth. From the doppler shift of the lines, the horizontal winds can be determined, while the line shapes and strengths yielded information about the temperature and atmospheric species such as mesospheric ozone. The reconstruction of a scattering density function from its integral over hyperbolas has also been developed [21] for wideband range-doppler radar imaging. Doppler imaging of a planar surface, however, has not been found to be studied in its own right.

D. ANALOGY BETWEEN HRR SAR AND HDR SAR

To illustrate the concept of obtaining a High Doppler Resolution (HDR) SAR image, a simplified explanation of the process of how a SAR image from high range resolution (HRR) is discussed, and an analogy will be drawn between the more common HRR SAR process, and the proposed process using HDR methods.

1. Image Formation Based on HRR Data

Traditional methods of imaging radars reply on high range resolution techniques to map out an image of the target. With one-dimensional high range resolution profiles, as discussed in Chapter II, the range profile of a target can be mapped. Given a sufficiently narrow time-domain pulse (relative to the major scatterers of the target), the relative locations of the scatterers can be differentiated to produce the range profile of the

target. One main issue with this simple concept is to address the scenario where the multiple scatters are located at the same distance from the radar. In such a scenario, all the scatterers will reflect energy back to the radar at the same time, and a single range profile will not be able to distinguish any cross-range structure. With a single set of range-only data, it will be almost impossible to make conclusive decisions pertaining to the nature of the target.

In order to build upon the information available from a range profile so as to extend the radar imaging concept to two dimensions, it is necessary to collect multiple sets of range profiles (each from different directions), process them, and finally synthesize an image. This process of building a two-dimensional image from multiple one-dimensional range profiles is similar to the idea of triangulation.

Consider a set of three simple point targets with the radar located relative to the target such that target 2 and target 3 are equidistant from the radar, as shown in Figure 14. The return signal to the radar will only indicate two targets in this configuration. If the radar is aboard a moving platform, and the platform moves directly towards the targets, the return signal will continue to indicate only two targets. This illustrates the condition where ambiguity exists due to targets lying along the lines of constant range from the radar.

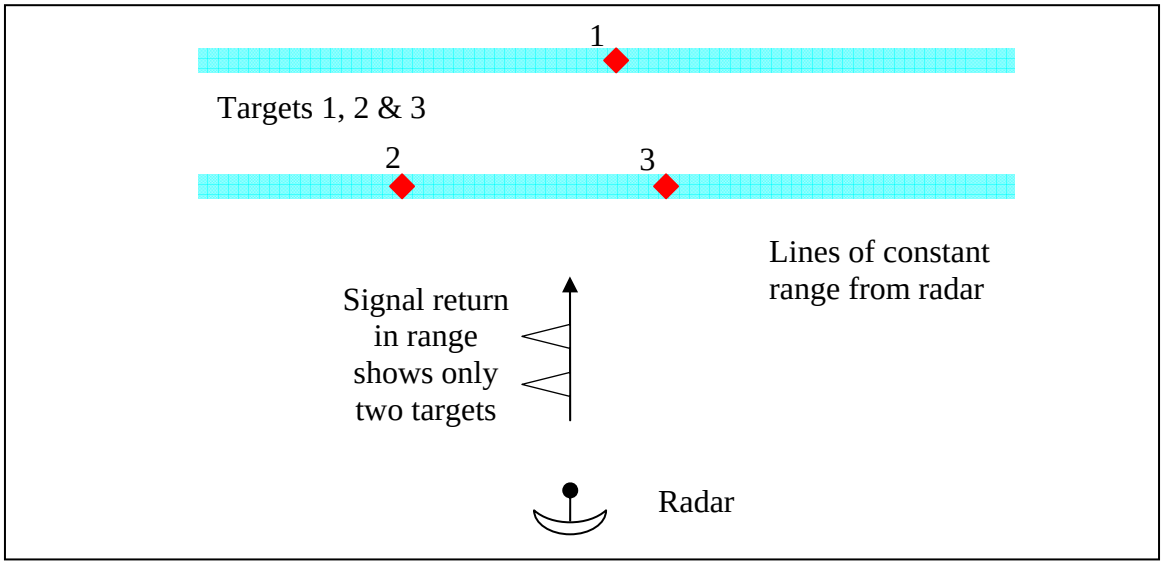

Figure 14 Ambiguity scenario due targets lying on lines of constant range from radar

However, if the platform has a component of velocity that is not parallel to the line-of-sight of the radar to the targets, the range profile will now start to show three targets. From a different perspective, the targets no longer line up along the same line of constant range, as shown in Figure 15. With multiple data sets from different directions, the concept of triangulation will allow the gradual buildup of the relative locations of the three targets using multiple sets of these one-dimensional range profiles. With the correct correlation methods (which will be discussed in the following sections), a two-dimensional image of the target as a whole can be obtained. Using just radial profiles, the cross-range information of the target has thus been obtained.

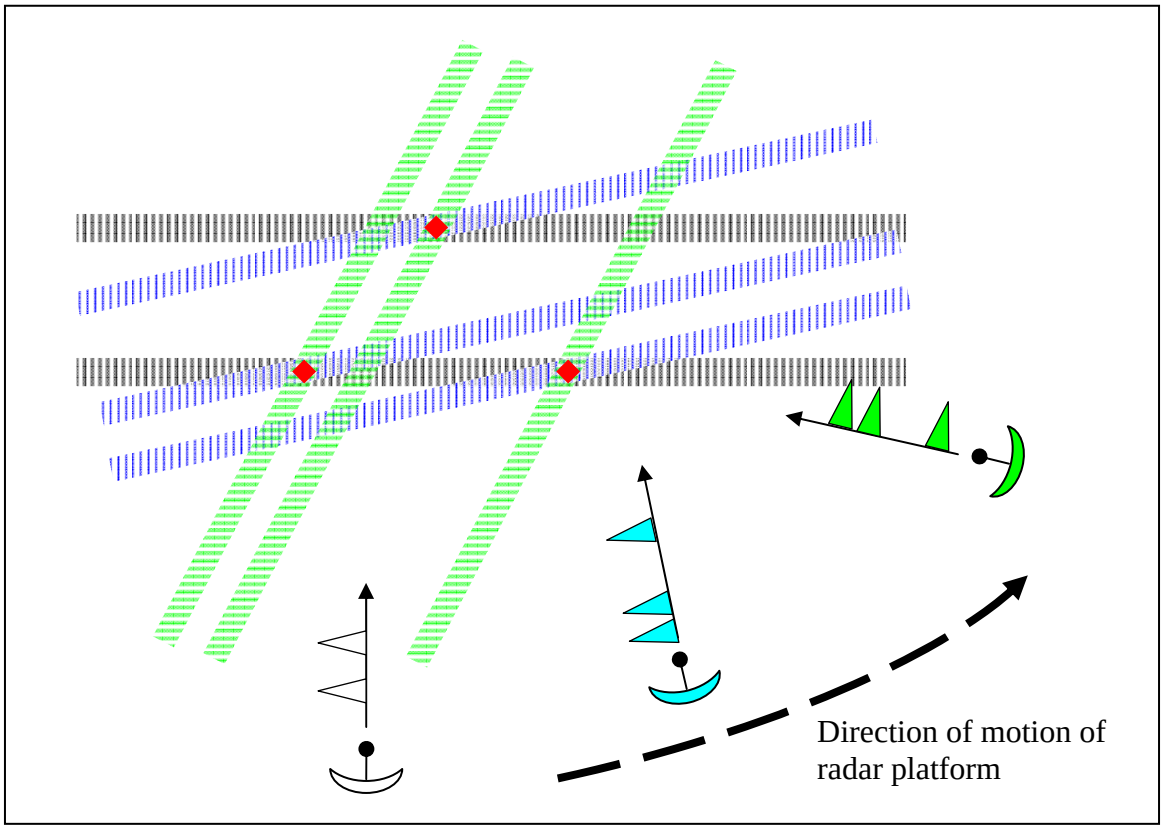

Figure 15 Down-range and cross-range information facilitates image reconstruction

Fundamentally, there are two different schemes used to collect target data from different perspectives (as described above) to obtain the cross-range information. The target can be stationary whilst the radar moves around the target to collect different range profiles of the target; or in the second scheme, the target is in motion whilst the radar is

stationary and stares at the target to collect a different perspective of the target. In the former case (where the radar is in motion), the radar is described as collecting data over a synthetically larger aperture, and thus termed as Synthetic Aperture Radar (SAR) as previously introduced in Chapter II. In the later case, the converse happens and the data is described as being collected by an Inverse Synthetic Aperture Radar (ISAR).

Mathematically, the basics for image formation are essentially the same for both cases (this will be shown in Chapter IV for the case of a basic rotating target). However, the details of data processing, such as correcting for departures from ideal target behavior, will be different in each setting, and thus there is still a need to differentiate the two processes.

2. Image Formation Based on HDR Data

The above section focused on how to synthesize an image based on high range resolution inputs for the case of a moving-radar-stationary-target case, and the complementary case of stationary-radar-moving-target case. This section will draw an analogy from the above described process to illustrate the concept utilizing high doppler resolution inputs to synthesize an image of the target.

In high range resolution SAR, the image is built up by a correlation of range profiles taken at different locations. Each “line” of the range profile is an iso-range line at a specific time that actually originates from the fact that the radar pulse takes a finite amount of time to reflect off a scatterer and return to the receiver.

In high resolution doppler, another set of “lines” can be used to build up the image. These will be the isodopplers as previously discussed, lines of constant doppler shift at a specific frequency based on the relative motion between the target and the radar. The return at a given doppler shift is a superposition of all the returns due to scatterers with the same relative velocity lying along the isodoppler hyperbola. Conceptually, iso-range lines and isodoppler lines can be thought of as taking “slices” of the image, and the difference between the former and the latter is that these “slices” are orthogonal to each other, as illustrated in Figure 16. Similar to the HRR scenario, there will be ambiguities

due to multiple scatterers along isodoppler, and thus doppler profiles of the target from different perspectives are required. Subsequent correlation of the data sets of doppler profiles will allow reconstruction of the image.

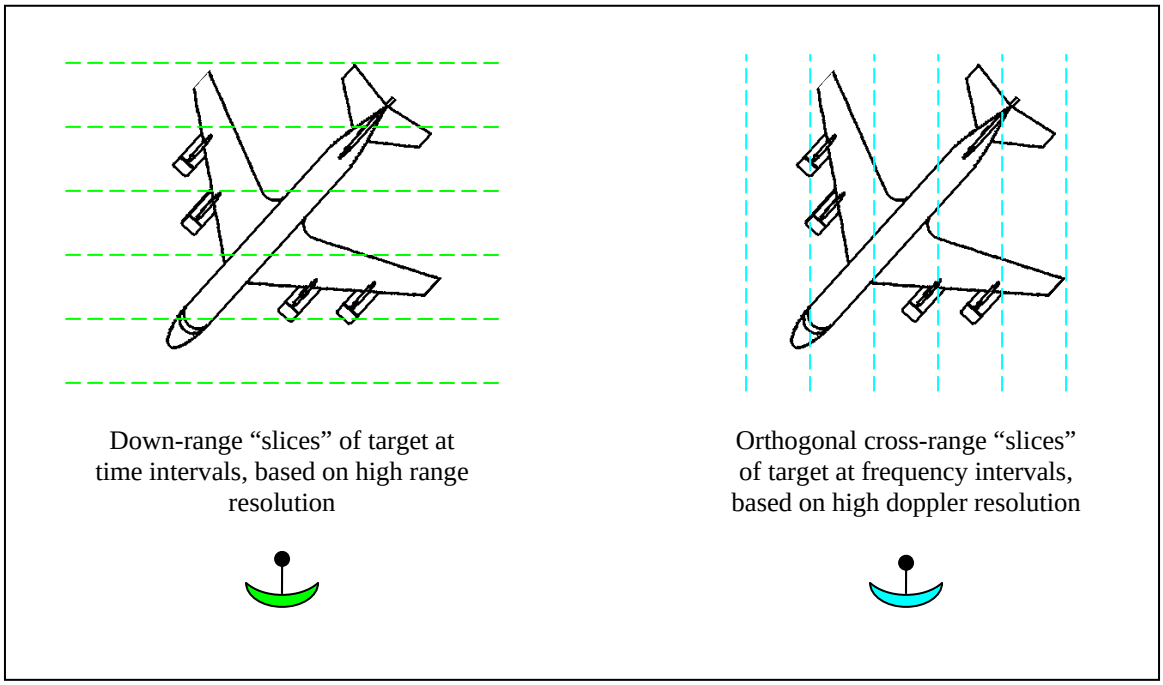

Figure 16 Different "slices" of the target when using HRR (left) and HDR

When imaging is based on high range resolution data, each profile will inherently have high resolution in the down-range direction, and the correlation of each profile from different perspectives will provide the cross-range resolution in order to build up a two dimensional picture. Conversely, when imaging is based on high doppler resolution data, each profile will have high resolution in the cross-range direction, and the correlation process will provide the down-range resolution. These are the underlying concepts of SAR based on doppler-only data.

E. MATHEMATICAL APPROACH TO HDR SAR

This section will broadly discuss the mathematical concepts [23] required to generate the SAR image based on high doppler resolution data. The specific implementation of these concepts and theorems will be discussed in Chapter IV.

1. Radon Transform and Tomography

A line integral represents the integral of some parameter of an object along a line. Taking the case of the radar and target scenario, the line integral represents the total reflection of the electromagnetic wave as it travels in a straight line to the target and back from it.

Consider a target represented by a two-dimensional function f(x,y), and line integrals defined by the parameters (τ,θ) as shown in Figure 17. Let the equation of line AB be $x\cos\theta + y\sin\theta = \tau$. For a fixed θ, there can be many possible other lines A'B' that are parallel to AB, each corresponding to a different value of τ. The line integral of along AB is defined as:

$$\Re_\theta(\tau) = \int_{\theta,\tau} f(x,y)ds$$

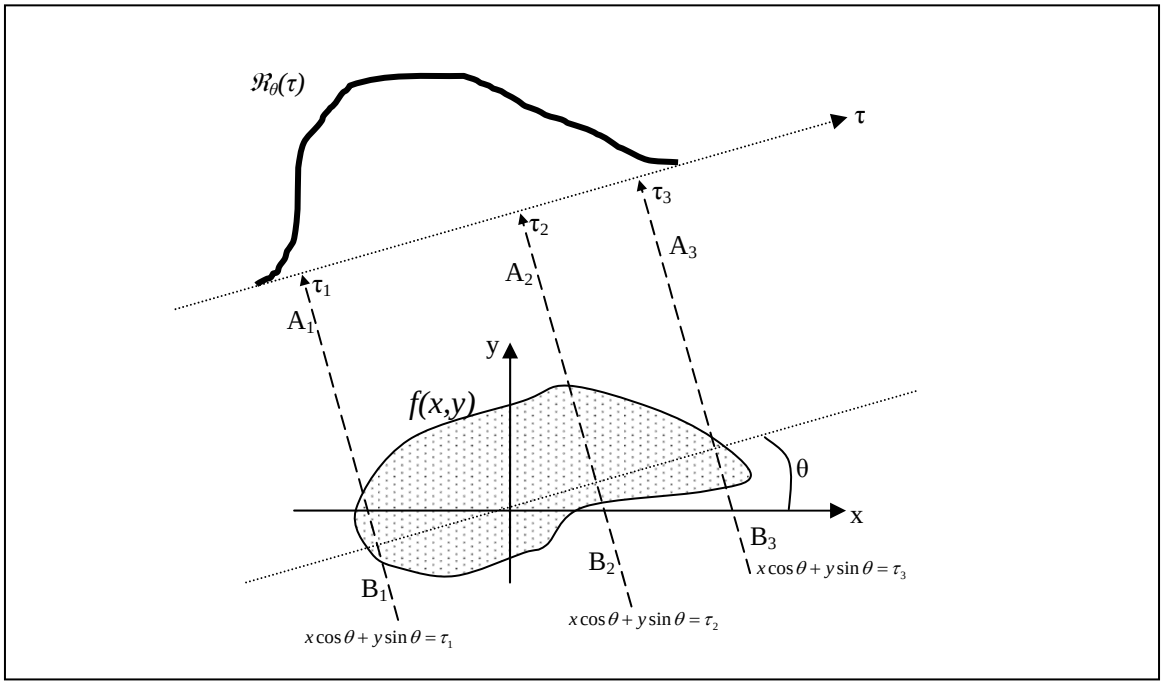

Figure 17 Concept of Line Integrals and the Radon Transform

Consider the delta function $\delta(\tau - x\cos\theta - y\sin\theta)$. This function is zero everywhere except when its argument is zero, which is along the straight line $x\cos\theta + y\sin\theta = \tau$. It is thus a representation of the line AB. Thus, the above function can be rewritten as:

$$\Re_\theta(\tau) = \int_{-\infty}^{\infty}\int_{-\infty}^{\infty} f(x,y)\delta(\tau - x\cos\theta - y\sin\theta)dxdy$$

$\Re_\theta(\tau)$ is known as the Radon transform of the function *f(x,y)*.

If θ is kept fixed at value θ_1 while τ is varied, then $\Re_\theta(\tau)$constitutes the projection of the density function *f(x,y)* onto the line $\theta = \theta_1$ as a function of τ. The resulting profile is referred to as a single scan. A projection of the function *f(x,y)* is formed by combining a set of line integrals. For a constant θ, the collection of parallel ray integrals forms a projection as shown in Figure 18.

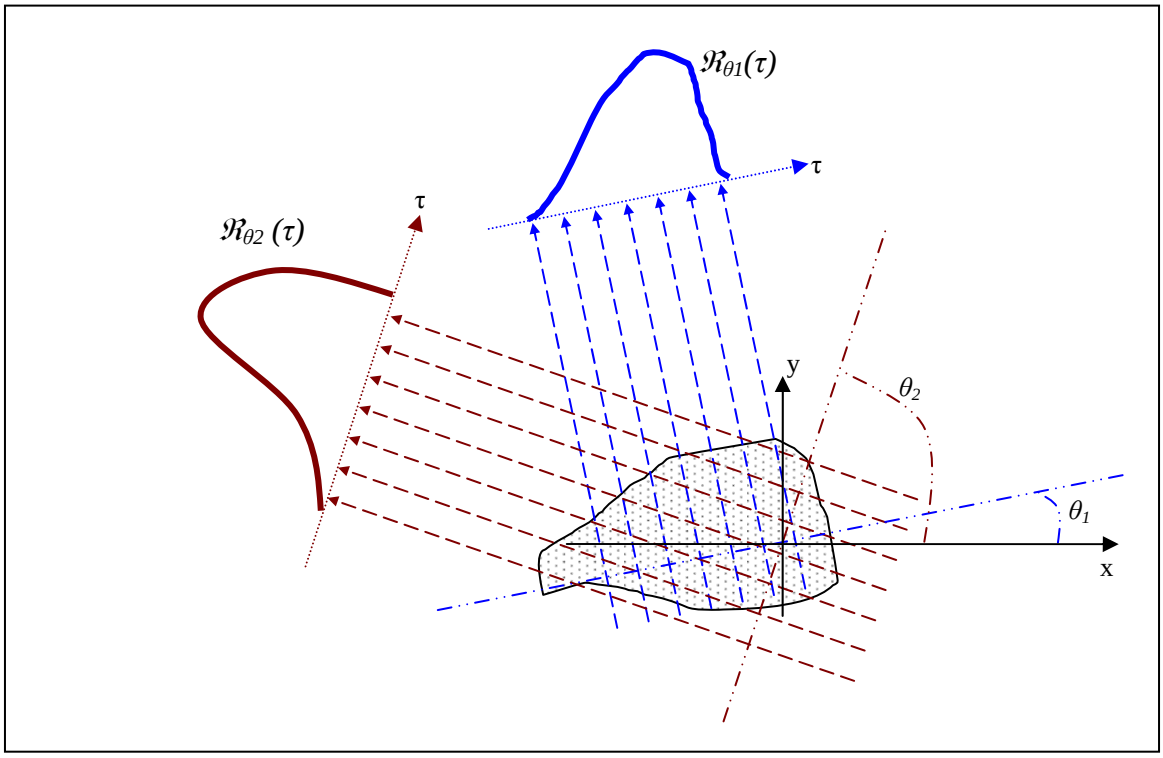

Figure 18 Radon Transform of *f(x,y)* based on Parallel Projections

The function *f(x,y)* is a representation of the reflectivity of the target, and the Radon transform of the target represents the superposition of all the returns due to scatterers with the same relative velocity lying along the isodoppler. The Radon transform data is often called sinogram because the Radon transform of a delta function is the characteristic function of the graph of a sine wave. Consequently, the Radon transform of a group of point scatterers making up the target appears graphically as a number of blurred sine waves with different amplitudes and phases.

Given the scans $\mathcal{R}_\theta(\tau)$, usually for continuous τ and a discrete set of scanning directions θ obtained by looking at the target from different perspectives, the aim is to invert this transformation so as to arrive back at the unknown target function *f(x,y)*. This concept is similar to computer-assisted tomography that is used in the medical field of CAT scans and magnetic resonance imaging.

2. Projection Slice Theorem

The two-dimensional Fourier transform of a function is defined as:

$$F(u,v) = \int_{-\infty}^{\infty}\int_{-\infty}^{\infty} f(x,y)e^{-i2\pi(ux+vy)}dxdy$$

Likewise, for a projection at an angle θ and the corresponding $\mathcal{R}_\theta(t)$, its Fourier transform is given by:

$$\Im(w) = \int_{-\infty}^{\infty} \Re_\theta(t)e^{-i2\pi wt}dt$$

Consider *F(u,0)*, the slice through *F(u,v)* along the *u*-axis given by setting $v = 0$ in the two-dimensional Fourier transform definition, to get:

$$F(u,0) = \int_{-\infty}^{\infty}\left[\int_{-\infty}^{\infty} f(x,y)dy\right]e^{-i2\pi ux}dx$$

From the definition of a parallel projection, it is noted that the item in square brackets is the projection of *f(x,y)* onto the *x*-axis, i.e.,

$$\int_{-\infty}^{\infty} f(x,y)dy = \Re_{\theta=0}(x)$$

Thus, $F(u,0) = \int_{-\infty}^{\infty} \Re_{\theta=0}(x) e^{-i2\pi ux} dx$

$$F(u,0) = \Im_{\theta=0}(u)$$

From the above equation, we see that the result is independent of the orientation between the object and the coordinate system. If the coordinate system is rotated by an angle θ, the Fourier transform of the projection is equal to the two-dimensional Fourier transform of the object along a line in the *u*-*v* plane, which is also rotated by an angle θ.

The Projection Slice Theorem states that the Fourier transform of a parallel projection of an image *f(x,y)* taken at an angle θ gives a slice of the two-dimensional transform, *F(u,v)*, subtending an angle θ with the *u*-aixs in the *u*-*v* plane. In other words, the Fourier transform of $\Re_\theta(\tau)$ gives the values of *F(u,v)* along the line τ' in the u-v plane. This is shown graphically in Figure 19.

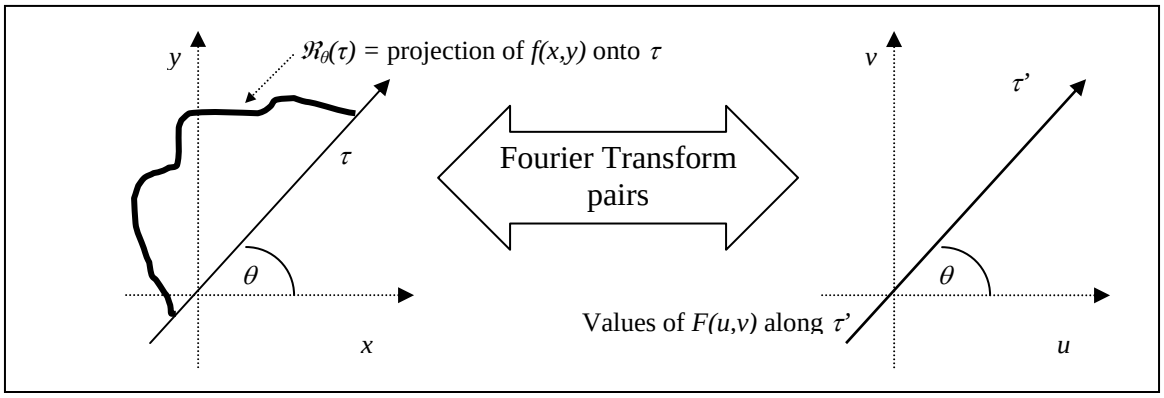

Figure 19 Graphical illustration of Projection Slice Theorem

3. Reconstruction by Filtered Backprojection

The Projection Slice Theorem relates the Fourier transform of a projection to the Fourier transform of the object along a single radial. Thus, given the Fourier transforms of projections taken at different angles, these projections could be assembled into a complete estimate of the two-dimensional transform, and then simply inverted to arrive at an estimate of the object. Conceptually, this provides a simple model of tomography, but practical implementations require a different approach.

The algorithm that is currently used for most applications of straight ray tomography is the Filtered Backprojection algorithm [25]. It has been shown to be accurate and amenable to fast implementation.

There are two steps involved in the Filtered Backprojection algorithm. The filtering portion can be visualized as a simple weighting of each projection in the frequency domain; the backprojection portion is equivalent to finding the elemental reconstruction corresponding to each of the filtered projections mentioned above.

The process of tomography is to project a certain $f(x,y)$ at various angles θ, which are preferably numerous and equally spaced. Consequently, those parts of the transform $F(u,v)$ can be deduced to lie on slices at corresponding angles. From knowledge of $F(u,v)$, one can recover $f(x,y)$ by a two-dimensional Fourier transform. It is noted that in the u-v plane, the data points resulting from various one-dimensional transformations lie on diverging spokes of constant θ. The density of points is thus inversely proportional to the radius, a nonuniformity that can be corrected for by multiplication with a weighting function. This is the rationale for the weighting process described in the first step of the Filtered Backprojection algorithm. The exact form of this weighting function will be discussed in the next chapter where the detailed implementation is discussed.

The final reconstruction is achieved by adding together the two-dimensional inverse Fourier transform of the weighted projection. As each projection only gives the values of the Fourier transform along a single line, this inversion can be performed very fast. This step is called a backprojection since it can be perceived as the smearing of each filtered projection back over the image plane.

In summary, based on the high doppler resolution data collected at different perspectives, the target image can be obtained by the following procedures:

- Extract the frequency components of the signal to obtain the sinogram (i.e., determine the Randon transform $\Re\theta(\tau)$ of the image).
- Fourier transform the projections to obtain $\Im\theta(\tau')$.
- Multiply $\Im\theta(\tau')$ by a weighting function.
- Sum over the image plane the inverse Fourier transforms of the filtered projections to obtain the reconstructed image.

THIS PAGE INTENTIONALLY LEFT BLANK

IV. IMPLEMENTATION OF DOPPLER IMAGING

Based on the doppler-only SAR concept introduced in the previous chapter, a procedure for implementation will be described and presented in this chapter based on a simple test scenario.

A. SCENARIO SETUP

Consider the case of an aircraft flying a circular path around *O*, of radius R_0 at a constant speed V_0. Its angular speed along the circular path is Ω_0, where $\Omega_0 = V_0 / R_0$. Within this circle lies a fixed target at a distance R_T from the centre of the aircraft's flight path. The angle subtended between the aircraft and the target with respect to the centre of the circular flight path is θ. The axis system is chosen such that the origin of the *x*-*y* axis is always with respect to the aircraft itself. Thus, the *y*-axis always points towards the centre of the circular flight path, *O*. The aircraft carries a continuous wave radar transmitting at a frequency f_0. This configuration is shown below in Figure 20.

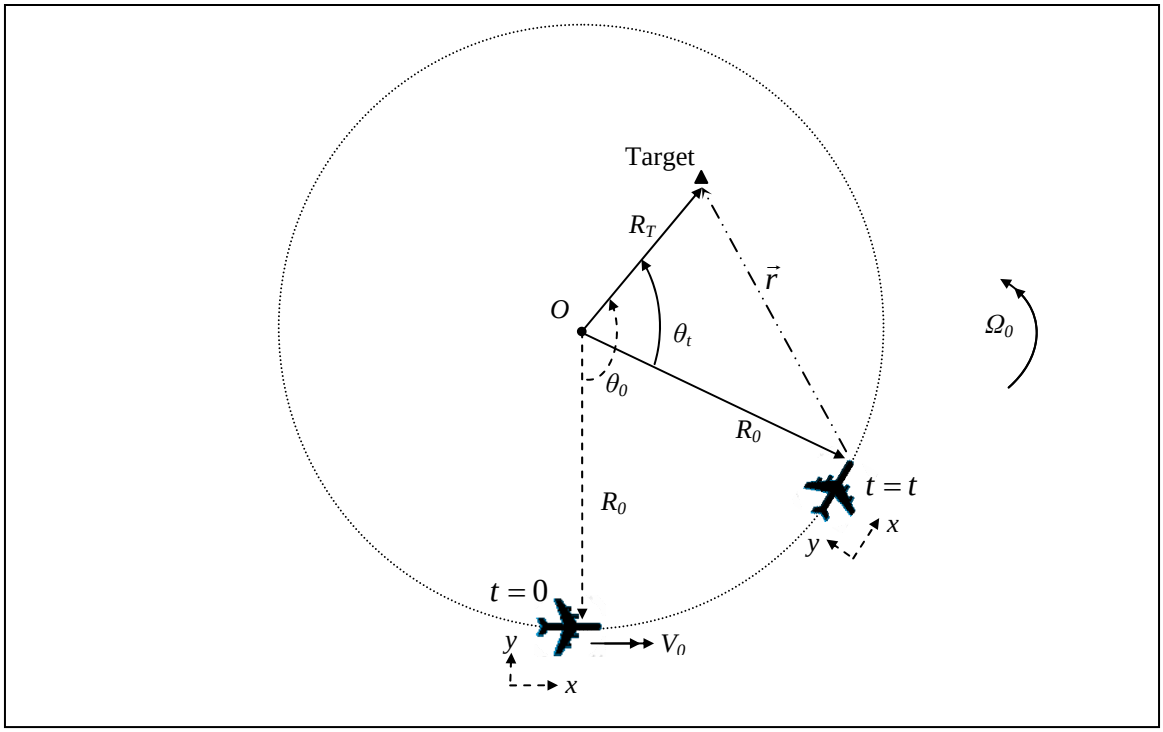

Figure 20 Aircraft flying a circular path enclosing a non-centered target at time *t*

Suppose at time $t = 0$, the angle subtended between the aircraft, the centre of the circular flight path, and the target is θ_0. Therefore, at time *t*, the angle subtended between the aircraft and the target is:

$$\theta_t = \theta_0 - \Omega_0 t$$

With the axis system centered on the aircraft itself, and if $\hat{\mathrm{x}}$ and $\hat{\mathrm{y}}$ are the unit vectors along the *x*- and *y*- axis respectively, then the position of the target with respect to the aircraft is:

$$\vec{r}_t = \left(R_T \sin\theta_t\right)\hat{\mathrm{x}} + \left(R_0 - R_T \cos\theta_t\right)\hat{\mathrm{y}}$$

If $\hat{\mathrm{r}}$ is the unit vector along $\vec{\mathrm{r}}$, then the position of the target with respect to the aircraft along $\hat{\mathrm{r}}$ is:

$$\vec{r} = \left[\sqrt{\left(R_T \sin\theta_t\right)^2 + \left(R_0 - R_T \cos\theta_t\right)^2}\right]\ \hat{r}$$

Differentiating $\vec{\mathrm{r}}$ with respect to *t*, we get $\vec{v}_r$, the velocity of the target with respect to the aircraft along $\vec{\mathrm{r}}$, where $\vec{v}_r$ is:

$$\vec{v}_r = \frac{d\vec{r}}{dt} = \frac{1}{2}\left[\left(R_T \sin\theta_t\right)^2 + \left(R_0 - R_T \cos\theta_t\right)^2\right]^{-\frac{1}{2}} \times$$
$$\left[2\left(R_T \sin\theta_t\right)\left(R_T \cos\theta_t\right)\left(-\Omega_0\right) + 2\left(R_0 - R_T \cos\theta_t\right)\left(R_T \sin\theta_t\right)\left(-\Omega_0\right)\right]$$
$$= \frac{-\Omega_0 R_T R_0 \sin\theta_t}{\sqrt{\left(R_T \sin\theta_t\right)^2 + \left(R_0 - R_T \cos\theta_t\right)^2}}$$

Since $\vec{v}_r$ is already the radial component of velocity between the target and the aircraft, the doppler shift resulting from the relative motion between these two objects are directly attributed to the full magnitude of $\vec{v}_r$.

Note that in this scenario, the aircraft and radar are moving, and the target is stationary. This essentially prescribes a SAR case where the imaging radar is in motion and the target is stationary. As mentioned in Section D of Chapter III, it will now be shown that mathematically there is an equivalent ISAR scenario to the SAR one just described above.

For an ISAR imaging system with a stationary radar and rotating target, consider the following scenario. A radar is located a distance of R_0 away from the centre of rotation of the target, O. The target is rotating with a radius R_T, and the speed of rotation is Ω_0, where the direction of rotation is clockwise as shown in Figure 21.

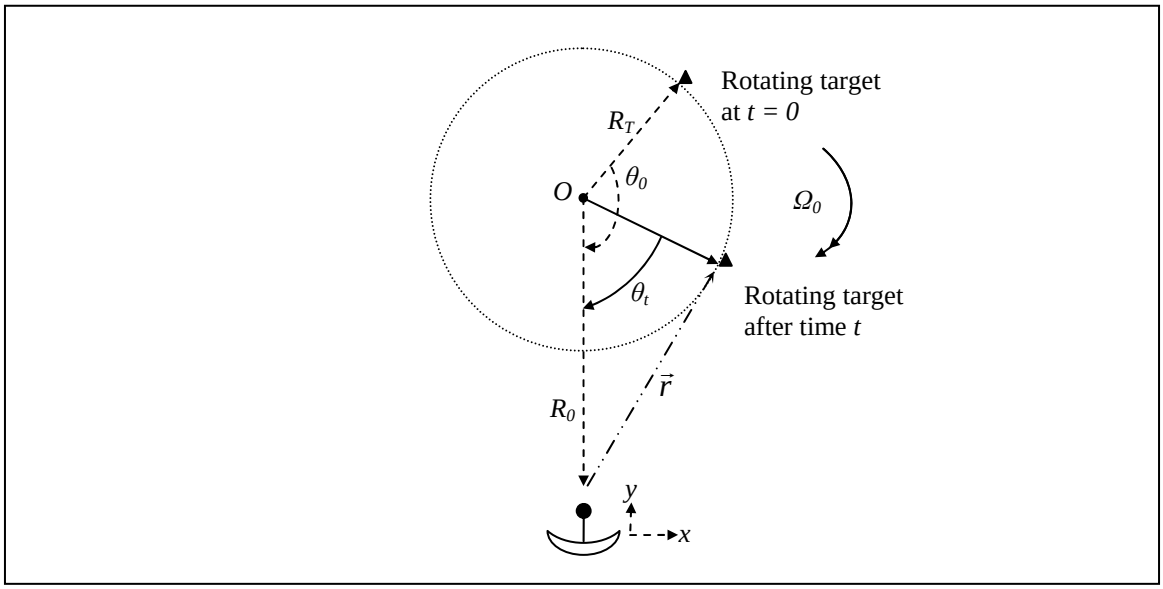

Figure 21 ISAR scenario, which is mathematically similar to the SAR one in Figure 20.

Suppose at time $t = 0$, the angle subtended between the radar, the centre of the rotating target, and the target itself, is θ_0. Therefore, at time t, the angle subtended between the aircraft and the target is:

$$\theta_t = \theta_0 - \Omega_0 t$$

An axis system is chosen whereby the origin is stationary, and is located at the position of the radar. With such an axis system, and if $\hat{\mathrm{x}}$ and $\hat{\mathrm{y}}$ are the unit vectors along the x- and y- axis respectively, then the position of the target with respect to the radar is

$$\vec{r}_t = \left(R_T \sin\theta_t\right)\hat{\mathrm{x}} + \left(R_0 - R_T \cos\theta_t\right)\hat{\mathrm{y}}$$

With the exception of the direction of rotation of Ω_0, the expressions for θ_t and $\vec{r}_t$ are exactly identical for both the SAR and ISAR scenario described above.

B. SIGNAL ANALYSIS FOR DOPPLER-ONLY SAR

In the previous section we derived expressions for $\vec{r}$ and $\vec{v}_r$ relating the positional and kinematic properties of the target from the radar for both the SAR and ISAR case (which have also been shown to be geometrically similar based on the described scenarios). Based on the doppler relationships discussed in Chapter III, the round trip doppler frequency shift, $f_{doppler}$, due to the relative motion of the radar and target is:

$$f_{doppler} = \frac{2v_r}{\lambda} = \frac{-2\Omega_0 R_T R_0 \sin\theta_t}{\lambda\sqrt{(R_T \sin\theta_t)^2 + (R_0 - R_T \cos\theta_t)^2}}$$

where λ is the wavelength of the transmitted frequency.

Since the doppler-only system uses a continuous wave radar transmitting at a constant frequency f_0, the received signal frequency f due to the doppler shift is:

$$f = f_0 + f_{doppler}$$

Due to a single scatterer target, the phase shift of the system will be given by $e^{i2\pi ft}$. For the case of multiple scatterers, it is noted that each scatterer will have a corresponding $R_{T,k}$ and $\theta_{0,k}$, thus contributing to a frequency shift of $f_{dopper,k}$. The combined signal, s_N, that is received by the radar due to the doppler shift of N scatterers is:

$$s_N = \sum_{k=1}^{k=N} A_k e^{i2\pi f_k t}$$

where $f_k = f_0 + f_{doppler,k}$

C. EXTRACTING THE RADON TRANSFORM OF THE TARGET

The SAR scenario described has assumed a circular rotational motion of the radar imaging a fixed target consisting of multiple point scatterers, which can be modeled by delta functions in space. The analysis also applies for the ISAR case with the only difference being an opposite direction of rotation. When the radar moves with a circular rotational motion, the superposition of the target from the different perspectives is

mathematically equivalent to a Radon transform of the target. This Radon transform of the target represents the superposition of all the returns due to scatterers with the same relative velocity lying along the isodoppler.

However, the received signal, s_N, in the form described above is not the Radon transform of the target yet. The Radon transform of a group of point scatterers making up the target appears graphically as a number of blurred sine waves with different amplitudes and phases. The Radon transform data is often called sinogram. The sinogram is actually a three-dimensional plot where the *x*- and *y*- axis are of *frequency* and *time*, and the *z*-axis indicates the relative magnitude of the value of that particular *frequency* at a particular *time*. In order to extract this sinogram from the signal s_N, a Short-Time Fourier Transform (STFT) will be performed on the signal. A short description of the STFT process is given below.

1. Short-Time Fourier Transform

Fourier analysis is not well suited to describing local changes in "frequency content" because the frequency components defined by the Fourier transform are taken over an infinite time, i.e., the Fourier transform assumes the signal is analyzed over an infinite time duration. Thus, Fourier transforms do not clearly indicate how the frequency content of a signal changes over time. To analyze the frequency content, one approach is to cut the signal into blocks and compute the spectrum of each block. This process, the "Short-Time Fourier Transform," is a Fourier-related transform used to determine the sinusoidal frequency and phase content of local sections of a signal as it changes over time [24].

The function to be transformed is multiplied by a window function, which is non-zero for only a short period of time. The Fourier transform (a one-dimensional function) of the resulting section of the signal is taken as the window is slid along the time axis, resulting in a two-dimensional representation of the signal. Mathematically, this is written as:

$$STFT\left\{s_N[\ ]\right\} = S_N(\tau, w) = \int_{-\infty}^{\infty} x(t)w(t-\tau)e^{-i\omega t}dt$$

The function *w(t)* is the window function, such as a Hamming or Gaussian window, and s_N is the function to be transformed.

In the discrete time case, the data to be transformed are broken up into smaller sets, which usually overlap each other, and each set is Fourier transformed. Mathematically, this is represented by:

$$STFT\left\{s_N[\ ]\right\} = S_N(m,w) = \sum_{n=-\infty}^{\infty} x[n]w[n-m]e^{iwn}$$

For both the continuous and discrete case, each frequency spectrum will show the frequency content during the short time, and so the successive spectra will show the evolution of frequency content with time.

Some of the parameters involved in setting up a STFT include the block length, the type of window, and the amount of overlap between blocks. In general, the result of the STFT process can be improved by choosing blocks that are overlapping, and multiplying each block by a window that is tapered at its endpoints.

One of the issues of STFT is that it has a fixed resolution. The width of the windowing function relates to the how the signal is represented. This determines whether there is good frequency resolution or good time resolution. A wide window gives better frequency resolution but poor time resolution; a narrower window gives good time resolution but poor frequency resolution.

2. Illustration of STFT with Sinusoidal Signals

A set of data consisting of sinusoidal signals will be used to illustrate the concept of STFT. The signal contains four different frequencies (500, 100, 110, 150 Hz), but in each time only one of the four frequencies are present. The signal is represented by:

$$x(t) = \begin{cases} \sin(2\pi 500t), \text{for} \quad 0 \le t < 1 \\ \sin(2\pi 100t), \text{for} \quad 1 \le t < 2 \\ \sin(2\pi 110t), \text{for} \quad 2 \le t < 3 \\ \sin(2\pi 150t), \text{for} \quad 3 \le t < 4 \end{cases}$$

The sinogram of *x(t)* is shown in Figure 22. The parameters used for this were a wide time window of 128 ms, but with two sets of overlap conditions. A second sinogram was also plotted with a narrow time window of 16 ms, and shown in Figure 23.

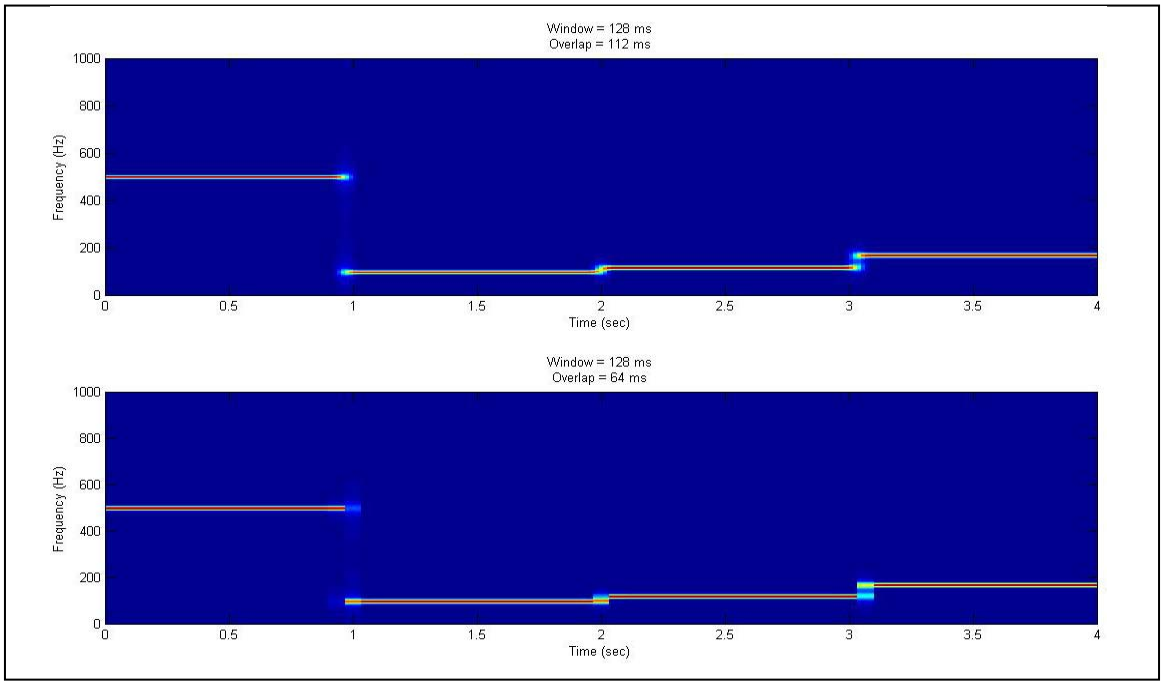

Figure 22 Sinogram of signal *x(t)* with a wide window and high frequency resolution

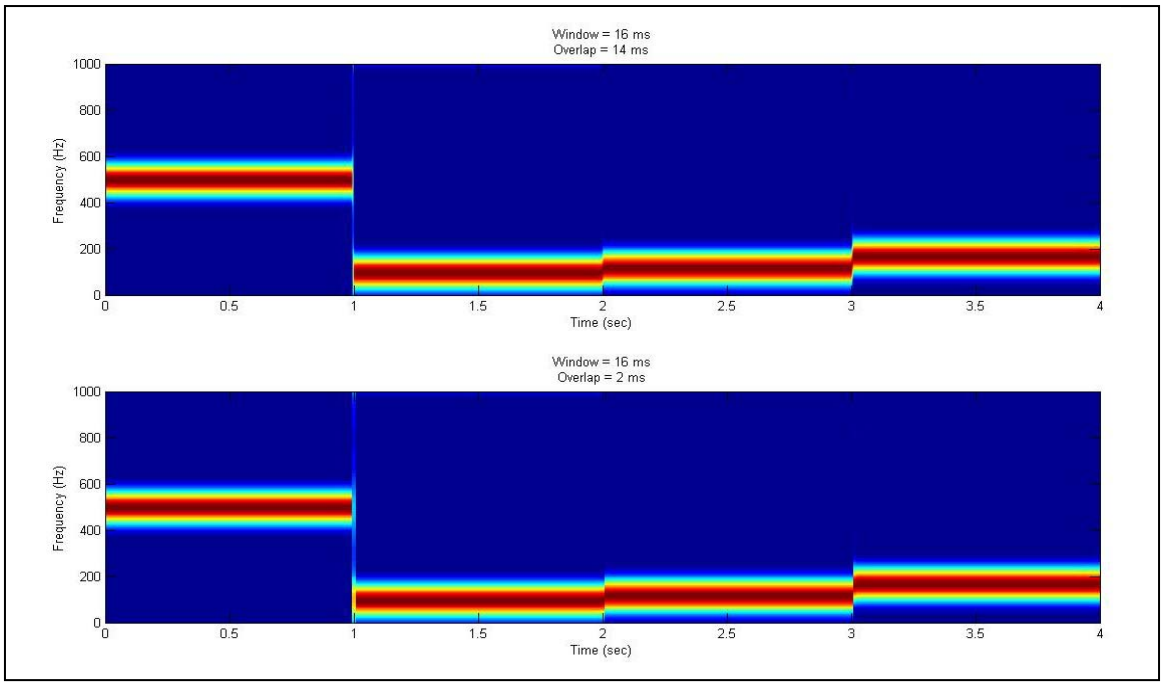

Figure 23 Sinogram of signal *x(t)* with a narrow window and high time resolution

As expected, a wide time window yielded a better frequency resolution, and a narrow time provided better time resolution. Also, a greater amount of overlap generally provides better resolution in frequency and time, and this is especially evident when comparing the crossover regions of the wide time window sinogram at frequency 100Hz to 110Hz from time 2 to 3 sec.

3. Sinogram of a Delta Function

It is useful to analyze the Radon transform of a delta function. The Radon transform of a function *f(x,y)* is defined as:

$$\Re_\theta(\tau,\theta) = \int_{-\infty}^{\infty}\int_{-\infty}^{\infty} f(x,y)\,\delta(\tau - x\cos\theta - y\sin\theta)\,dxdy$$

This following analysis is significant as, in the sequel, the target is assumed to be made up of a composition of individual scatterers, and each scatterer is modeled with a delta function.

Consider two delta functions located at $(x_1,\ y_1)$ and $(x_2,\ y_2)$, then $f(x,y) = \delta(x-x_1)\delta(y-y_1) + \delta(x-x_2)\delta(y-y_2)$, and:

$$\begin{aligned}\Re_\theta(\tau,\theta) &= \int_{-\infty}^{\infty}\int_{-\infty}^{\infty}\left[\delta(x-x_1)\delta(y-y_1) + \delta(x-x_2)\delta(y-y_2)\right]\delta(\tau - x\cos\theta - y\sin\theta)\,dxdy \\ &= \delta(\tau - x_1\cos\theta - y_1\sin\theta) + \delta(\tau - x_2\cos\theta - y_2\sin\theta) \\ &= \delta(\tau - r_1\sin(\theta-\phi_1)) + \delta(\tau - r_2\sin(\theta-\phi_2))\end{aligned}$$

where $r_n = \sqrt{x_n^2 + y_n^2}$, and $\phi_n = \arctan\left(-\frac{y_n}{x_n}\right), n = 1, 2.$

The above shows that the Radon transform of a two point scatterers are a pair of sine curves, and that these curves are distinct from each other, as shown in Figure 25.

Assuming a grid of 100 x 100, delta functions are placed at different locations and the Radon transform of the “target” is plotted. The sinograms are shown in Figure 24.

It is noted that when a delta function is at the center of the grid (corresponding to a physical SAR scenario where the circular flight profile is directly centered on the target), the sinogram is a straight line. As the delta function is placed further from the

center of the grid, the amplitude of the sine wave increases. Depending on which side of the grid the delta function is placed (physically, this corresponds to the relative positions between SAR aircraft and the target), the phase of the sine wave is shifted accordingly. Although not immediately apparent from the figures below, the frequency of the sine wave is determined by the linear (or rotational) speed of the aircraft.

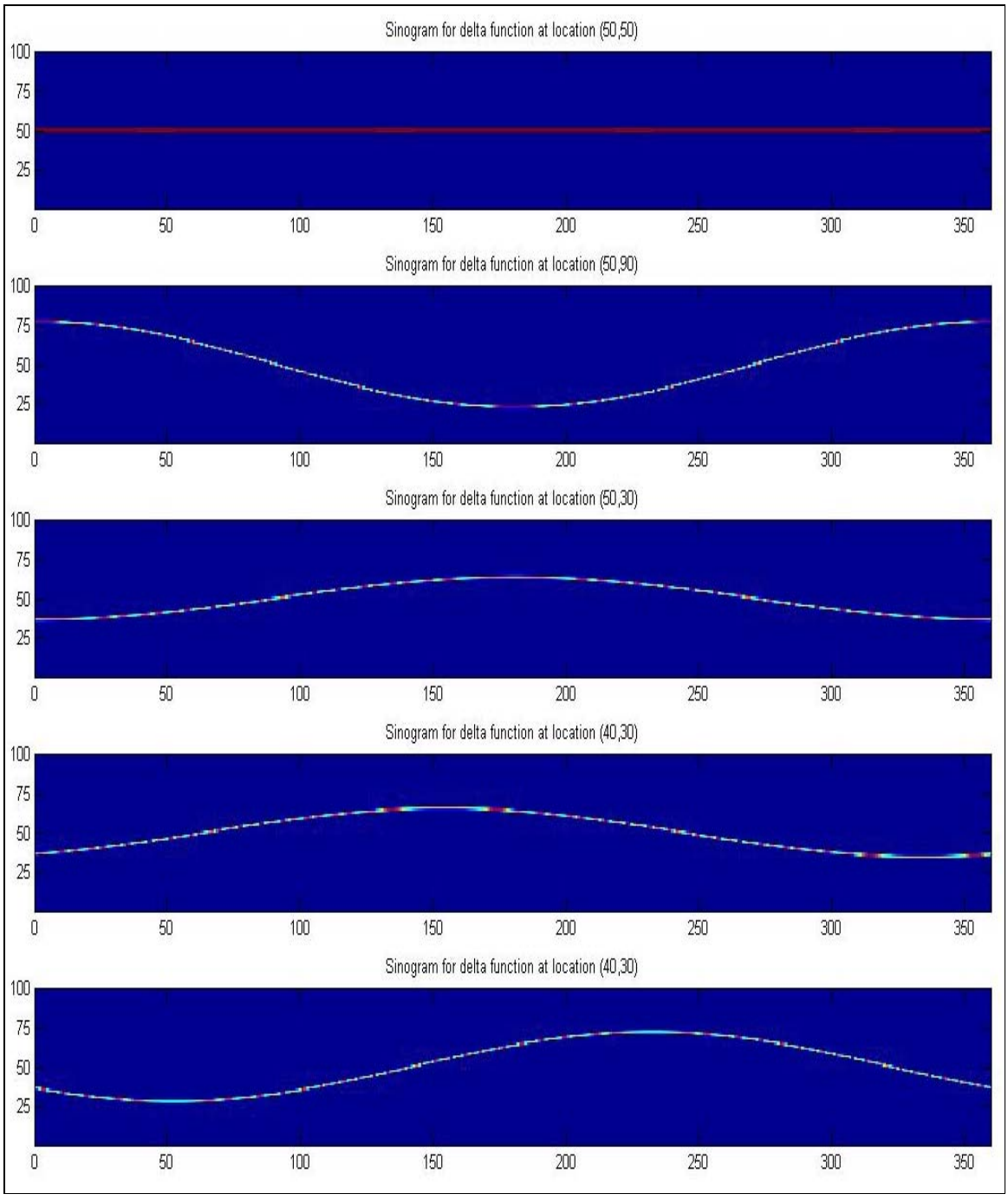

Figure 24 Sinograms of delta functions at various locations on a 100x100 grid

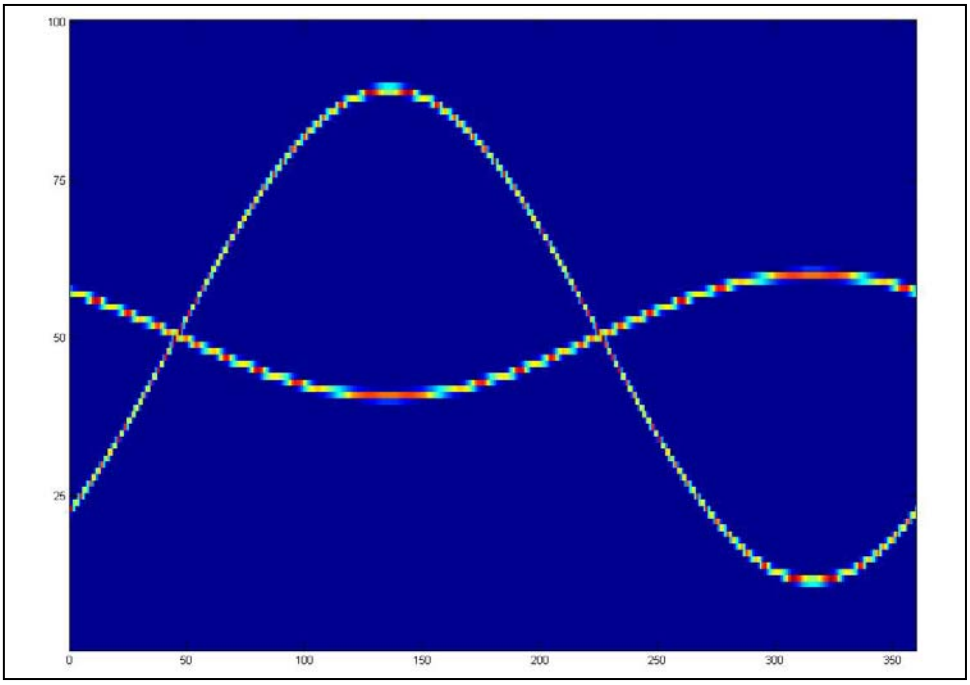

Figure 25 Sinograms of a pair of delta functions at (10,10) and (60,60)

In summary, a Short-Time Fourier Transform is performed on the received signal, s_N, to obtain S_N, which corresponds to the Radon transform of the target. Since the Radon transform of a delta function is a sine wave, and if the target is assumed to be made up of discrete scatterers, each modeled by a delta function, then the Radon transform of the target will be a sinogram consisting of a series of sine waves with different phases and amplitudes. An Inverse-Radon transform process, which is the subject of the next section, is then applied to the sinogram in order to reconstruct an image of the target.

D. INVERSE-RADON TRANSFORM

Chapter III gave a brief introduction to the Inverse-Radon process, implemented via the two-step Filtered Backprojection method, as a means to reconstruct the image of the target from the sinogram. The first step is a filtering process, which can be visualized as a simple weighting of each projection in the frequency domain. The second step is the backprojection process, which is the successive addition of the filtered projections in the appropriate coordinates in the *x*-*y* plane, thereby obtaining a reconstruction of the original image. These two steps will be further elaborated in the following sections.

1. Filtering Process

Recall that the Fourier Slice Theorem relates the projection of the image along a line in the time domain to another line in the Fourier domain via a Fourier transform. Consider a single projection and its Fourier transform. If the values of the Fourier transform of the projection are inserted into their proper place in the object's two-dimensional Fourier domain, then a simple reconstruction (based on only one set of projections) had effectively been performed.

It is noted, however, that in the *u*-*v* plane, the data points resulting from various one-dimensional transformations lie on diverging spokes of constant θ. When the projections are collected in the *u*-*v* plane, sampling rates (or in the case when numerical simulation is used, the discrete FFT points) result in data points being evenly spaced along that particular spoke. This is illustrated in Figure 26. This results in a high concentration of data points at the centre of the *u*-*v* plane. The density of the radial points becomes sparser as the distance from the centre increases.

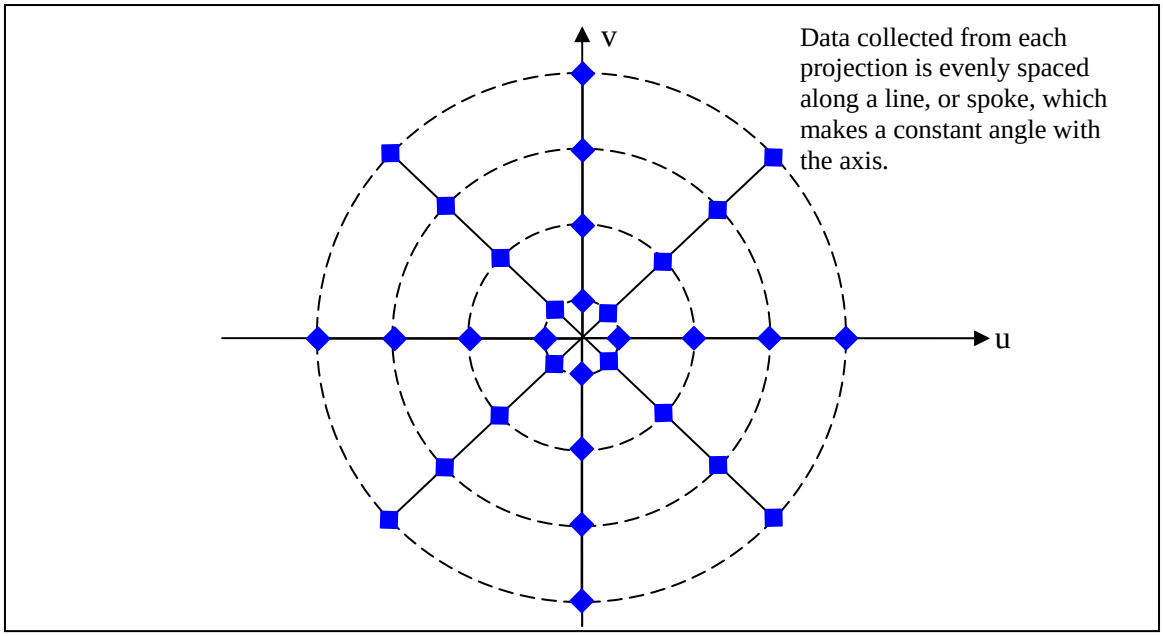

Figure 26 Data points evenly spaced along a spoke result in higher density of points near the centre

Therefore, the aim of the filtering process can be thought of as applying appropriate weights to the data collected in order to account for the differing densities at different locations based on their radial distance from the centre. It is expected that the

weighting function should have a smaller value when close to the centre and a relatively larger value when the distance from the centre increases. Keeping in mind that the projections are taken over a frequency *w*, it turns out that the weighting factor is simply $|w|$. This will be shown mathematically in the subsequent section, where the factor of $|w|$ actually represents the Jacobian for a change of variable between polar coordinates and the rectangular coordinates required for the Fourier transform [25]. The physical interpretation of the weighting factor is as explained above. The aim of this filtering process is to facilitate a simple reconstruction via the backprojection process, which is explained in the next section.

2. Backprojection Process

The final reconstruction is found by adding together the two-dimensional inverse Fourier transform of each of the weighted projections. Since each projection has been properly weighted, and gives only the values of the Fourier transform along a single line, the image reconstruction is a simple and even smearing of the filtered projection over the corresponding line in the image plane. The weighting process performed previously was to enable each projection to contribute evenly to all the pixels along the appropriate line AB in the *x-y* plane, as illustrated in Figure 27.

3. Mathematical Implementation of the Filtered Backprojection

The concept of the Filtered Backprojection process to implement an Inverse-Radon transform has been explained, and the mathematical implementation will now be presented.

Recall that for an inverse Fourier transform, the object function, $f(x,y)$, can be expressed as:

$$f(x,y) = \int_{-\infty}^{\infty}\int_{-\infty}^{\infty} F(u,v)e^{i2\pi(ux+vy)}dudv$$

A change of coordinate system from rectangular to polar is performed in the frequency domain, i.e., from (u,v) to (w,θ), by making the coordinate and differential substitutions:

$$u = w\cos\theta$$
$$v = w\sin\theta$$
$$dudv = \frac{\partial(u,v)}{\partial(w,\theta)}\,dwd\theta = |w|dwd\theta$$

The inverse Fourier transform of a polar function is thus:

$$f(x,y) = \int_0^{2\pi}\int_{-\infty}^{\infty} F(w,\theta)e^{i2\pi w(x\cos\theta + y\sin\theta)}|w|dwd\theta$$
$$= \int_0^{2\pi}\left[\int_{-\infty}^{\infty}|w|F(w,\theta)e^{i2\pi w(x\cos\theta + y\sin\theta)}dw\right]d\theta$$

This equation can be applied in the Filtered Backprojection process when the following substitutions for the terms in the square brackets are made:

$\tau = x\cos\theta + y\sin\theta$, the line about which the projection is taken, and

$F(w,\theta) = \Im_\theta(w)$, where $\Im_\theta(w)$ is the Fourier transform of $\Re_\theta(w)$

The resulting equation is:

$$f(x,y) = \int_0^{2\pi}\left[\int_{-\infty}^{\infty}|w|\Im_\theta(w)e^{i2\pi w\tau}dw\right]d\theta$$
$$= \int_0^{2\pi} Q_\theta(x\cos\theta + y\sin\theta)d\theta$$

where $Q_\theta(t) = \int_{-\infty}^{\infty}|w|\Im_\theta(w)e^{i2\pi wt}dw$, which is the inverse Fourier transform of $|w|\Im_\theta(w)$.

$|w|\Im_\theta(w)$ represents the filtered projection, and the physical explanation for multiplication by $|w|$ is the compensation for the decreasing density of data points as the distance from the centre increases. The resulting projections for different angles θ are then added to reconstruct an image of *f(x,y)*.

Thus, we have formed an estimation of $f(x,y)$ from the projection data $\mathcal{R}_\theta(\tau)$. The Filtered Backprojection algorithm is summarized as follows, and shown in Figure 27.

- The collected data from the change in doppler frequency is $\mathcal{R}_\theta(\tau)$
- $\mathcal{R}_\theta(\tau)$ is Fourier transformed to obtain $\mathcal{T}_\theta(\tau)$
- The filtered projection is multiplied by the weighting factor $|w|$, which behaves like a smoothing filter to compensate for the decreasing density of data points as the distance from the centre increases
- This weighted, filtered projection is backprojected evenly over the image plane along the appropriate line

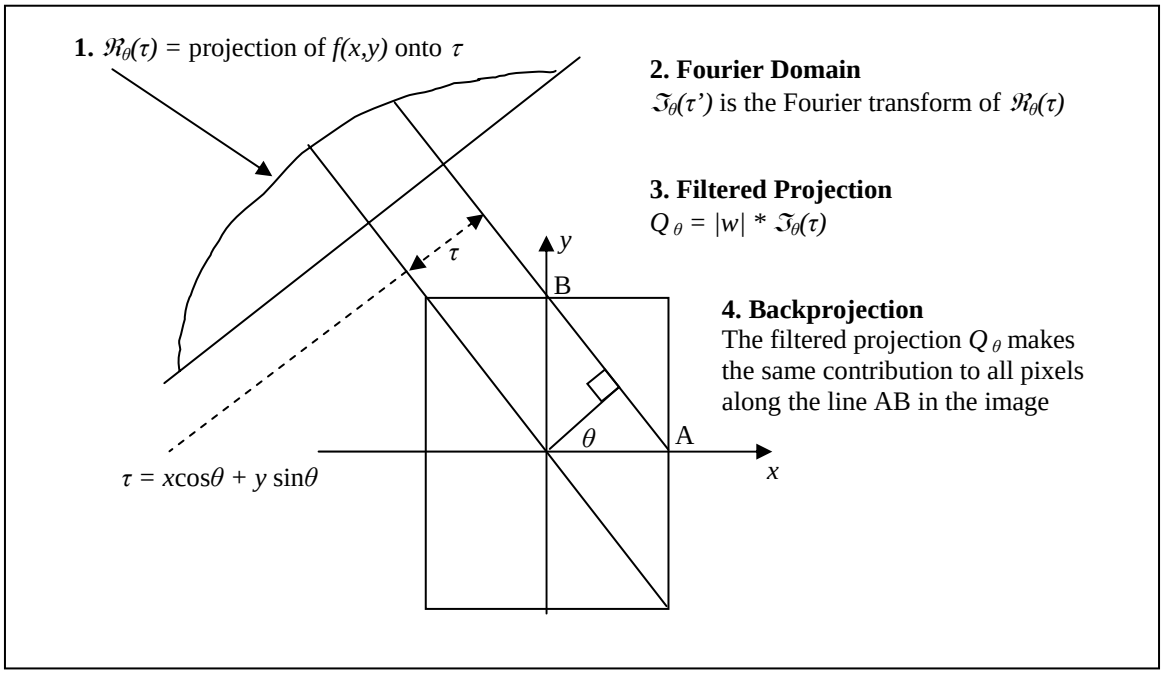

Figure 27 Overview of the reconstruction process (After [25])

V. RESULTS AND FUTURE WORK

A. RESULTS

The image reconstruction scheme using high-doppler resolution data, as described in Chapter IV, had been implemented based on the ISAR scenario shown in Figure 21. Using a simple target modeled by various sets of delta functions, the following reconstructed images were obtained.

1. Basic Reconstruction Results

A simple target modeled by three delta functions in a straight line used to check for generic accuracy of the implementation scheme. This is shown in Figure 28. The picture in the upper left corner is the reconstructed image of the original three delta functions. The other three remaining pictures show the locations of the individual delta functions if the original image had consisted of only one single delta function. A comparison of the images will indicate that the implementation scheme is able to distinguish each individual delta function and reproduce the correct image.

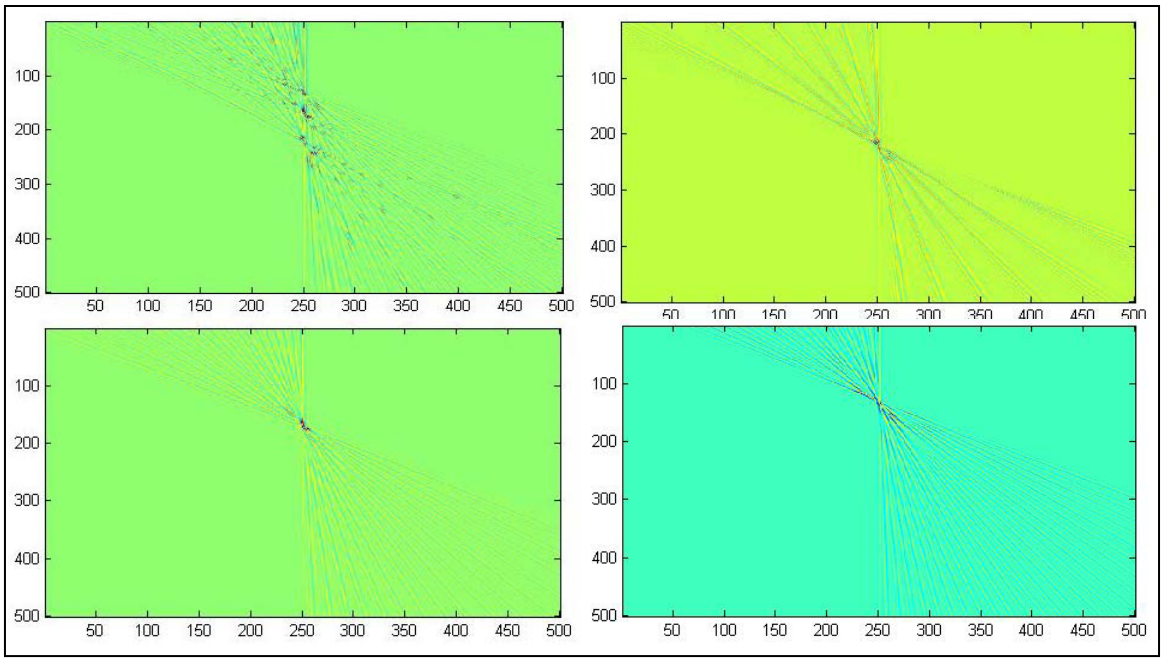

Figure 28 Image reconstruction of three delta functions in a straight line (upper left), and individual images of each of the three delta functions

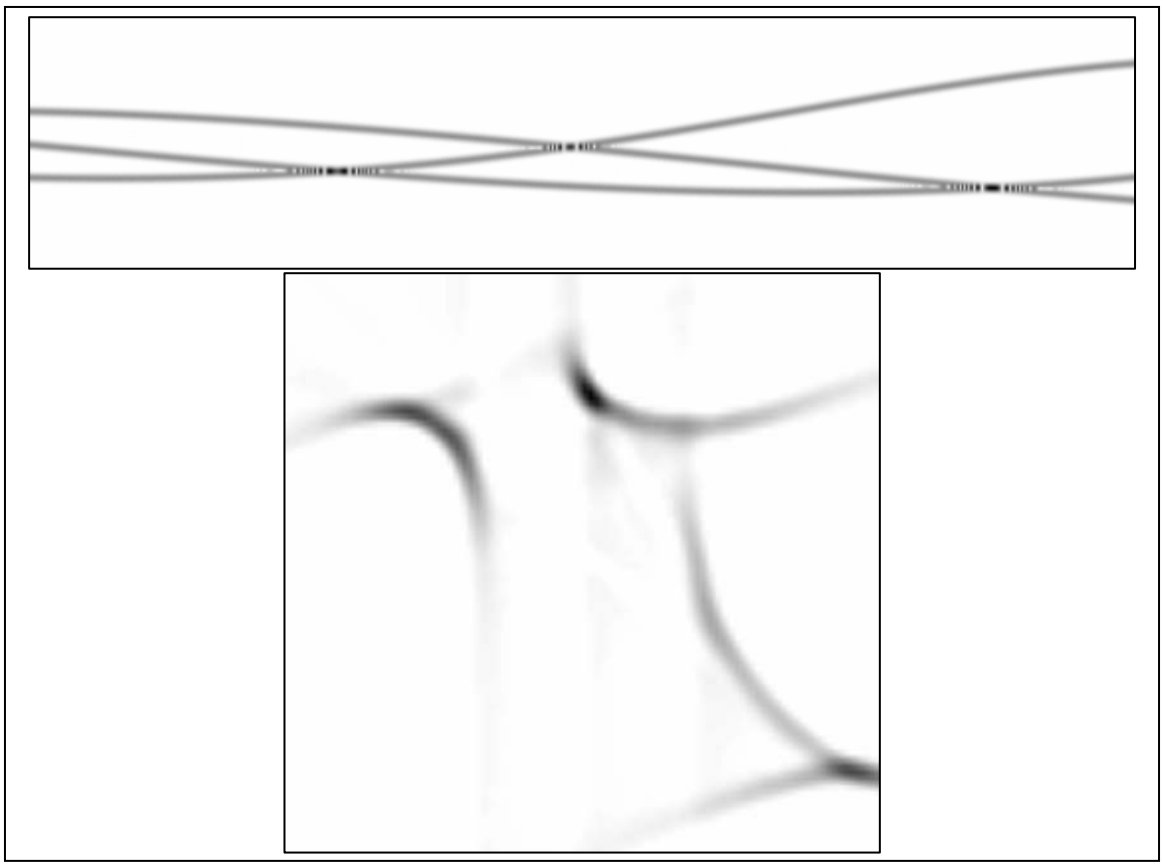

Figure 29 Sinogram (top) and reconstructed image of three point-scatterers

The sinogram and reconstructed image of a set of three delta functions is shown in Figure 29. It is also noted that the reconstructed image of each delta function is not a point image, but rather an area of finite size, and that there are “lines” of relatively smaller amplitude extending radially outwards from this point.

The next set of figures show the effects on quality of the image when a different number of “views” is taken of the target. Consider the simple case when the image is a single delta function at the centre of the circular flight path taken by the aircraft and radar in a SAR configuration. The reconstructed image when the aircraft flies 45°, 90°, 135° and 180° around the target are shown respectively (starting clockwise from top-left) in Figure 30. Examining the image when the aircraft flies 45° around the target, it can be seen that there are interference lines radiating from the centre of the target. Similar lines are found in each of the other three pictures such that it can be roughly estimated how much of a perspective the aircraft had taken of the target.

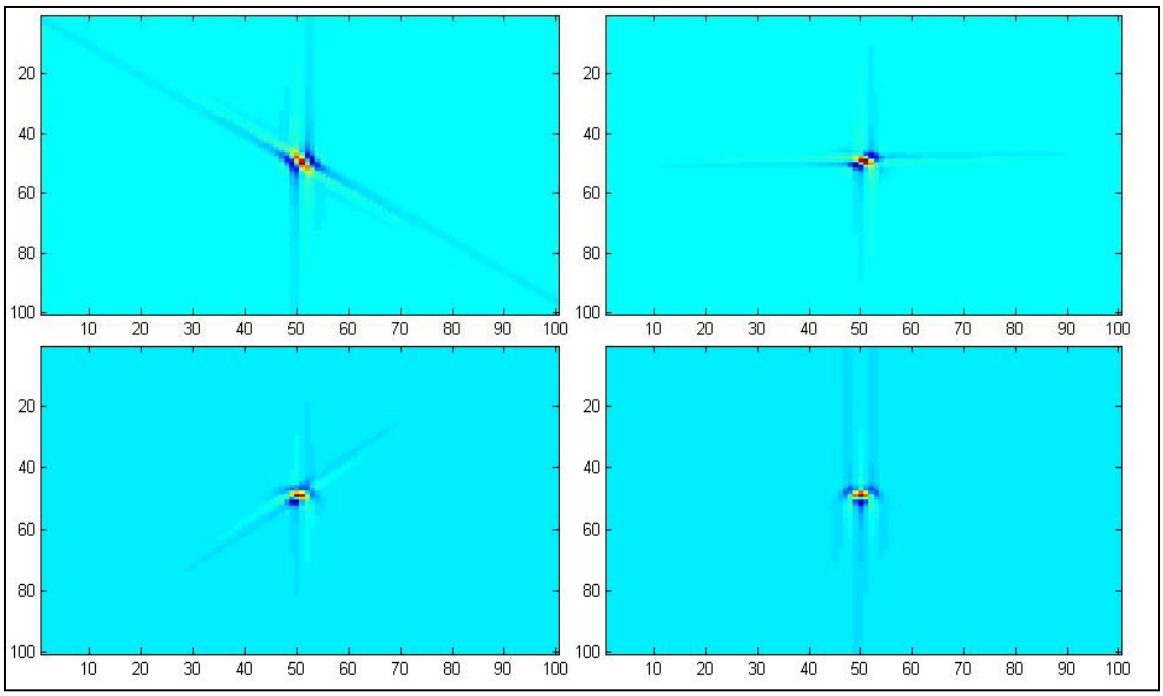

Figure 30 Image reconstruction based on 45°, 90°, 135° and 180° (starting clockwise from top-left picture) views of the target

Another analysis on the effects of taking a different number of perspectives of the target can be seen in Figure 31. When more perspectives are taken of the target, a clearer and better resolution image can be obtained.

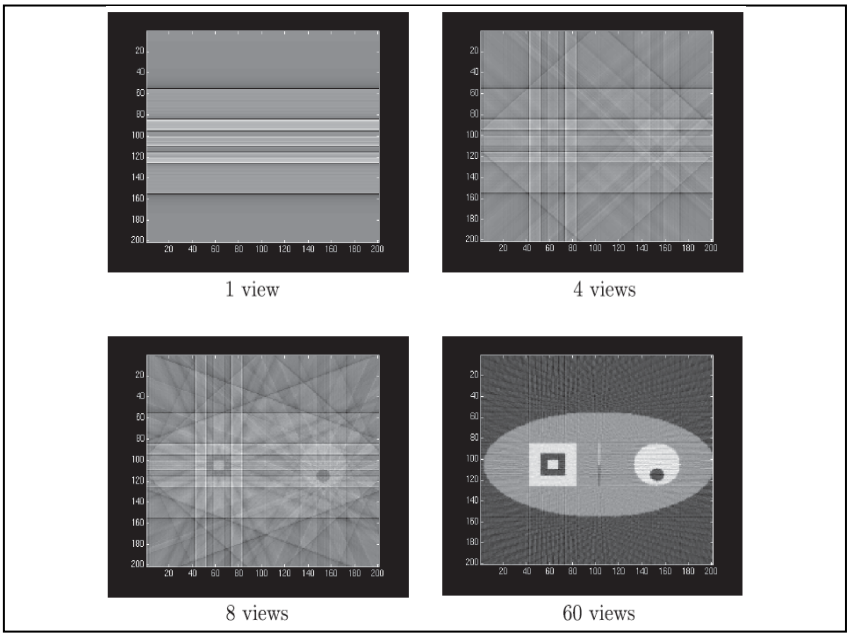

Figure 31 Effect of taking different number of perspectives of the target

2. Discussion of Results

The following were noted when analyzing the reconstructed images based on high-doppler resolution data.

Firstly, the reconstructed image produced a proportionately scaled representation of the image. The scaling factor depends on a variety of factors such as how the computational Fast Fourier Transform (FFT) was performed to evaluate Fourier transforms and inverse Fourier transforms, window and step sizes for the Short-Time Fourier Transform, and image size output parameters for the Filtered Backprojection algorithm. Thus, some reference on the length scale of the original image is necessary in order to correlate the scaled image with the real image.

Secondly, the number of “perspectives” or “views” of the target from the radar is an important factor is determining the quality of the reconstructed image. An analogy can be drawn with the process of triangulation. When the baselines for triangulation are large, an object location can be triangulated to a higher degree of accuracy. Similarly, when a larger number of perspectives are taken of the target, a better resolution of the image can be obtained.

Thirdly, it is noted that the reconstructed image of a delta function has another point of finite size, and that there are radial lines of comparatively smaller amplitude extending from that point. These lines represent some form of second-order interference patterns originating from the finite implementation (e.g., computational Fourier transforms) of high frequency components associated with delta functions. By themselves, these interference patterns are seen to be clearly of lower amplitude than the signal forming the image itself. However, when a more complex image consisting of multiple scatterers is analyzed, the interference lines from multiple scatterers may begin to form constructive interference and certain points, thereby giving rise to additional peaks in the reconstructed image. This phenomenon can be visualized by examining the above mentioned effects in Figure 28. Nevertheless, when an increasing number of views of the target are taken, the amplitude of the interference lines become progressively smaller so that any apparent images from points of constructive interference are not of significant amplitude, which can be as seen in Figure 30.

Finally, a simple resolution analysis for this doppler-only SAR implementation was performed. Based on simulation results, it was found that a resolution up to 30 units can be discriminated. When two delta functions are separate by about 30 units, the doppler-only image can just discern two separate images as shown in Figure 32.

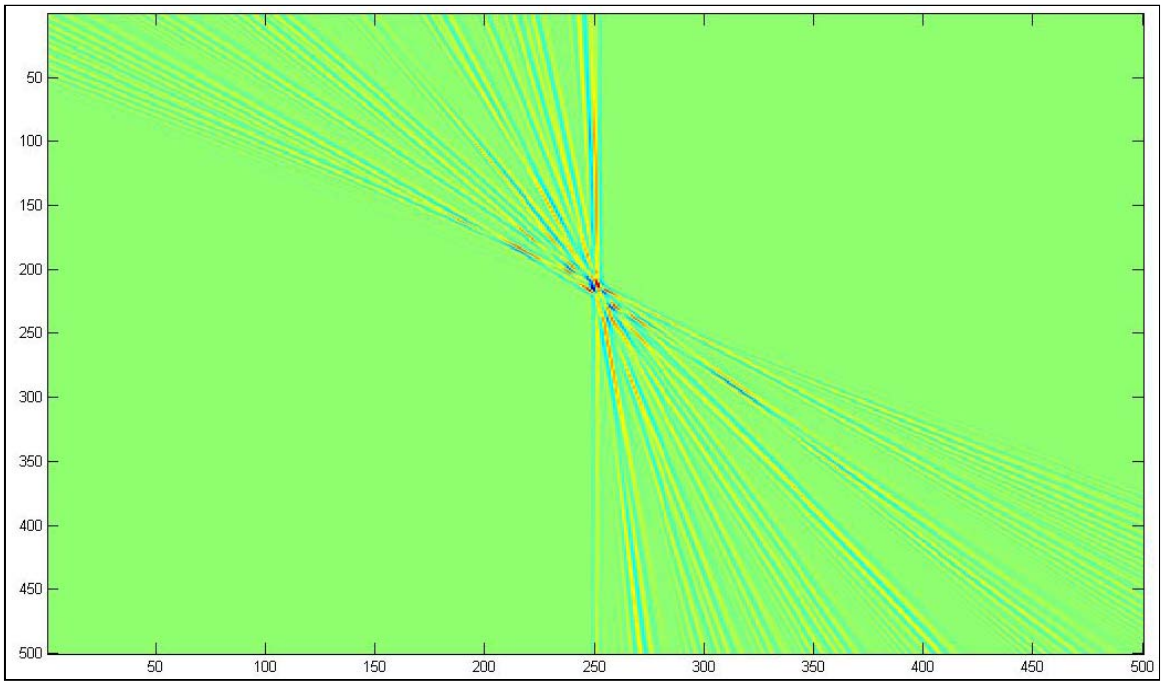

Figure 32 Resolution limit when delta functions are separated by 30 units

B. FUTURE WORK

1. More Complex Scenarios

The scenarios analyzed thus far have been based on simple objects modeled by individual delta functions, and based on simple two-dimensional geometry of SAR/ISAR configuration. Although this has been sufficient for proof-of-concept of utilizing high-resolution data for doppler-only SAR, this treatment is not sufficient for more complex image analysis.

Further analysis is found in [12], where a more generalized analysis of the doppler-only SAR is conducted with a three-dimensional perspective based on a straight flight path and flat Earth, and an efficient implantation scheme is proposed for higher

computational efficiency in reconstructing the image. Such a scheme can be tested more rigorously on complex data such as the DARPA “Backhoe Data Dome” backscatter data of a backhoe vehicle in free space.

2. Resolution Analysis

The current study has not included an analytical treatment for determining image resolution. In [12], a down-range and cross-range resolution computation has been proposed, and this could be tested and verified based on data from the Backhoe Data Dome. Resolution analysis will be critical to evaluate the feasibility of using high-doppler resolution data to perform radar imaging, as well as provide comparisons with current methods which are based on high-range resolution data.

3. Performance in Real Environment

The high-doppler resolution data both in this thesis and in the Backhoe Data Dome are simulated data in a noise-free environment. As with many other fields of conceptual studies, the difference between theoretical study and real-world performance may be a wide chasm. In the field of radar, field testing constitutes an important component towards fine tuning the performance of the radar due to the many significant factors that the environment plays. A practical test of the performance of the doppler-only SAR will be necessary to evaluate whether this concept is a viable alternative or suitable complementary system to existing high-range resolution systems in service today

VI. SUMMARY AND CONCLUSION

A. SUMMARY

Conventional SAR and ISAR have traditionally been performed using high-range resolution data. It is thus conceptually viable that such an imaging process can also be performed using high-doppler resolution data only. This thesis has been a proof-of-concept that such an imaging algorithm is possible.

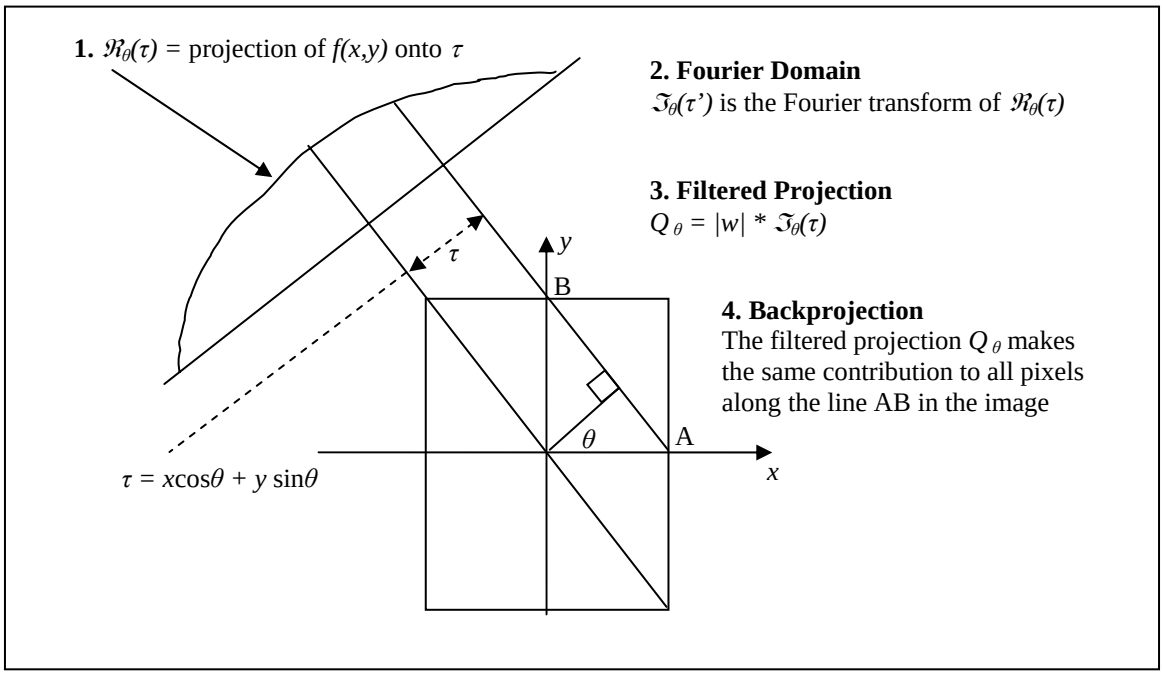

Figure 33 Summary of the image reconstruction process (After [25])

The physics behind the imaging process have been studied and presented. The process is summarized in Figure 33. For a SAR/ISAR scenario (which are mathematically similar), high-range resolution data are collected along an isorange line for different perspectives of the target. Similarly, for the doppler-only SAR concept, high-doppler resolution data is collected along an isodoppler line for different perspectives of the target. Mathematically, this data is equivalent to taking the Radon transform of the target (where projections of the target are taken along a line), and the resultant data is called a sinogram.

By the Projection Slice theorem, the Fourier transform of the sinogram from each perspective (for example, at an angle θ) gives a slice of the two-dimensional transform subtending an angle θ with the u-axis along the u-v plane. This process provides equally distributed points along a line subtending an angle θ with the axis. However, such a density distribution also results in a higher density of points near the centre (or origin), and a lower density of points as the distance from the centre increases. Some form of weighting, $|w|$, is thus applied to the Fourier transform of the sinogram, and mathematically this weighting of $|w|$ corresponds to the Jacobian when a coordinate transform is performed from the rectangular to polar form as part of the analysis.

The weighting factor described above can also be seen as a filtering process, and is part of the Filtered Backprojection algorithm to determine the Inverse Radon transform of the sinogram. The backprojection portion of the Filtered Backprojection algorithm is a simple and equal redistribution of points back along the original line upon which the original projections were taken.

Simple test cases consisting of images modeled by sets of delta functions were used to test the above described algorithm. The reconstructed images have been presented, and an initial analysis performed. The main points noted were:

- The reconstructed image was a scaled version of the original image, and the scaling factor was dependent on parameters used in the various computational processes such as the Fourier transform, STFT and Filtered Backprojection algorithm.
- As expected, the quality of the image improved when more perspectives of the target were taken.
- The image of each delta function was a finite point with interference patterns. In a complex target with multiple interference patterns, the constructive interference of these patterns at certain points may show up as ‘ghost’ images. However, when more perspectives are taken, the amplitude of each set of interference patterns decrease, and thus ‘ghosting’ effects would not be significant.

B. CONCLUSION

The concept of using high-doppler resolution data for doppler-only SAR has proven to be viable. This analysis can be further strengthened by considering a generalized analysis conducted from a three-dimensional perspective, testing based on more complex data, and performing better resolution analysis.

The impetus for developing a high-doppler resolution system is based on a relatively simpler transmitter design, smaller bandwidth requirements for use in covert operations, restrictive electromagnetic spectrum or mediums with narrow spectral windows, and possibly lower frequency operations for ground and foliage penetration imaging systems.

THIS PAGE INTENTIONALLY LEFT BLANK

APPENDIX

This appendix contains a Matlab program that generates a simulated high-doppler resolution signal, and implements the Doppler-Only SAR algorithm described in this thesis to reconstruct the original image.

```
%Matlab code for Doppler-Only SAR

clear all;

%-----Begin Section---------------------
% Variable Definition
f = 1e9;                %radar freq 1GHz
c = 3e8;                %speed of light
R0 = 1000;              %Range between radar and centre of rotation
v = 100;                %Linear speed of target
w = v / R0;             %Rotational speed

time_step = 0.001;

total_time = 20;

%total_time=total_time*4;

%-----End Section----------------------


%-----Begin Section---------------------
%Input data on scatterers, defined based on distance and angle from
centre
N = 3;                  %number of point scatterers

theta(1)=0*pi/4;        %these set of data is used to image a circle
R(1)=200;
theta(2)=2*pi/4;
R(2)=200;
theta(3)=4*pi/4;
R(3)=200;
theta(4)=6*pi/4;
R(4)=200;
theta(5)=1*pi/4;
R(5)=200;
theta(6)=3*pi/4;
R(6)=200;
theta(7)=5*pi/4;
R(7)=200;
theta(8)=7*pi/4;
R(8)=200;
%-----End Section----------------------
```

```
%-----Begin Section---------------------
%Generate signal
t = 0:time_step:total_time;

for n=1:N
    x = R(n).* cos (theta(n) + w.*t);
    y = R(n).* sin (theta(n) + w.*t) + R0;
    r = ( (x).^2 + (y).^2 ).^.5;
    velocity = 0.5.*(x.^2 + y.^2).^(-0.5) .* ( (2.*x.*-
R(n).*sin(theta(n) + w.*t).*w) + (2.*y.*R(n).*cos(theta(n) + w.*t).*w)
);
    doppler = 2*velocity/c*f;
    rx_freq = f + doppler;
    signal = exp(i*2*pi*rx_freq.*t);
    for index = 1: size(velocity,2);
%        v(n,index)=velocity(index);         %v,s,rx_f, s are 2-D
matrixes
%        d(n,index)=doppler(index);          %that contain the
indivdual
%        rx_f(n,index)=rx_freq(index);       %data for each scatterer
        s(n,index)=signal(index);
    end
%    figure(n);
%    plot (t,d(n,:),'b');                   %plot the curves
end

%Check to see if mathematical formula for differential of r is correct
via
%numerical differential

%for t1=1:size(t,2)-1
%    v2(t1) = (r(t1+1)-r(t1))/time_step;
%end
%figure(2)
%plot (v2,'k');

radon_data=zeros(1,size(s,2));
for n=1:N;
    radon_data=radon_data+s(n,:);       %radon_data is the combined
signal
end

%-----End Section----------------------

% perform short time fourier transform
%[extract_freq stft_parameters] = stft(radon_data,128,64,128,2);

windowsize=64;
[extract_freq,stft_parameters] = stft(radon_data,windowsize,32,64,2);
%[extract_freq,stft_parameters]= stft(radon_data);

%[extract_freq,stft_parameters]= stft(s(2,:));
%extract_freq= specgram(s(2,:));
```

```
% perform frequency shift so that there is no crossover data
for index=1:size(extract_freq,2)
    data_shift(:,index)=fftshift(extract_freq(:,index));
end

colormap(1-gray);
[nr,nc]=size(data_shift);

imagesc(abs(data_shift(1:nr,1:nc-windowsize)))

%perform inverse radon transform
%variable angle is based on the STFT window step size

angle = stft_parameters(2)*time_step*w/pi*180;
%irad=iradon(data_shift,angle,'linear', 'Hamming', 1, 500);
%irad=iradon(abs(data_shift(1:nr,1:nc-windowsize)),angle,'linear',
'Hamming');
irad=iradon(abs(data_shift),angle,'linear', 'Hamming');
imagesc(irad);
```

THIS PAGE INTENTIONALLY LEFT BLANK

LIST OF REFERENCES

[1] Skolnik, M.I., *Introduction to Radar Systems*, Second Edition, pp. 369-380, McGraw Hill, 2001.

[2] Cohen, M.N., "An Overview of Radar-Based, Automatic, Noncooperative Target Recognition Techniques," *IEEE International Conference on Systems Engineering*, pp. 29-34, 01 August 2001.

[3] Information Builders, *Decision Support Systems – DSS (definition)*, http://www.informationbuilders.com/decision-support-systems-dss.html, September 2006.

[4] Freeman, T., What is Imaging Radar?, http://southport.jpl.nasa.gov/desc/imagingradarv3.html, September 2006.

[5] Hudson, S., and D. Psaltis, "Corrrelation Filters for Aircraft Identification from Radar Range Profiles," IEEE Trans., AES-32, pp. 741-748, July 1993.

[6] Linde, G. J. and Platis, C. V., "Target Recognition with Surveillance Radar," Naval Research Laboratory Review, pp. 118-120, 1995.

[7] Sandia National Laboratories, Synthetic Aperture Radar Applications, http://www.sandia.gov/RADAR/sarapps.html, September 2006.

[8] Defence Research and Development Canada, Non-Cooperative Target Recognition of Air Targets (NCTR), http://www.ottawa.drdc-rddc.gc.ca/html/RAST-309-nctr_e.html, September 2006.

[9] Nathanson, F.E., Radar Design and Principles, Second Edition, McGraw Hill, 1980.

[10] Eaves, J. and Reedy, E., "Polarimetric Fundamentals and Techniques," Principles of Modern Radar, First Edition, Springer, 1987.

[11] Lipps, R. and Bottoms, M., "Polar Reformatting for ISAR Imaging," Naval Research Laboratory, http://www.nrl.navy.mil/content.php?P=02REVIEW124, October 2006.

[12] Borden, B., Cheney, M., "Synthetic-Aperture Imaging from High-Doppler-Resolution Measurements," Institute of Physics Journal on Inverse Problems, Vol. 21, No. 1, February 2005.

[13] Willis, N. J., Bistatic Radar, First Edition, SciTech Publishing, 2005.

[14] Kogon, S. and Zatman, M., “Bistatic STAP for Airborne Radar,” MIT Lincoln Laboratory, http://www.ll.mit.edu/asap/asap_00/procabs/kogan.htm, October 2006.

[15] Skolnik, M.I., Introduction to Radar Systems, Second Edition, pp. 339-369, McGraw Hill, 2001.

[16] Globalsecurity.org, Weapon of Mass Destruction (WMD) Yongbyon [Nyongbyon], http://www.globalsecurity.org/wmd/world/dprk/yongbyon-imagery.htm, November 2006.

[17] SRI International, Foliage Penetrating Radar – FPR Detection of Obscured Objects, http://www.sri.com/esd/penetratingradar/folpen/folpen.html, November 2006.

[18] Mercury Computer Systems, Black River Systems – Revealing Deep Dark Secrets, www.mc.com/literature/literature_files/blackriversys1-as.pdf, November 2006.

[19] Mensa, D. L., High Resolution Radar Imaging, Artech House, 1981.

[20] Upper Atmospheric Research Satellite, High Resolution Doppler Imager, University of Michigan - Space Physics Research Laboratory, http://hrdi.engin.umich.edu/index.html, November 2006.

[21] Maass, P., Wideband Radar: the hyp transform, Institute of Physics Journal on Inverse Problems, Vol. 5, No. 5, October 1989.

[22] Oliver, C. and Quegan, S., Understanding Synthetic Aperture Radar Images, SciTech Publishing, 2004.

[23] Bracewell, R. N., The Fourier Transform and its Applications, Third Edition, pp. 329-358, McGraw Hill, 2000.

[24] Wikipedia, Short Time Fourier Transform, http://en.wikipedia.org/wiki/Short_Time_Fourier_Transform, November 2006.

[25] Kak, A.C. and Slaney, M., Principles of Computerized Tomographic Imaging, IEEE Press, 1988.

[26] Roulston M. S. and Muhleman D. O., “Synthesizing radar maps of polar regions with a Doppler-only method,” Applied Optics, Vol. 36, Issue 17, pp. 3912-3919, 1997.

INITIAL DISTRIBUTION LIST

1. Defense Technical Information Center
   Ft. Belvoir, Virginia

2. Dudley Knox Library
   Naval Postgraduate School
   Monterey, California

3. Professor James H. Luscombe
   Code PH/Lj
   Naval Postgraduate School
   Monterey, California

4. Professor Brett Borden
   Code PH/Bb
   Naval Postgraduate School
   Monterey, California

5. Professor Donald L. Walters
   Code PH/We
   Naval Postgraduate School
   Monterey, California

6. Professor Phillip E. Pace
   Code EC/Pc
   Naval Postgraduate School
   Monterey, California

7. Professor Yeo Tat Soon
   Director, Temasek Defence Science Institute
   National University of Singapore
   Singapore

8. Tan Lai Poh
   Senior Admin Officer (MDTS), Temasek Defence Science Institute
   National University of Singapore
   Singapore

9. Cheng Lock Charles Chua
   Ministry Of Defence
   Singapore